



POLITECNICO DI TORINO

Master degree course in Biomedical Engineering

Master Degree Thesis

Ultrasounds scans of Inferior Vena Cava in pneumological patients

Supervisors

Prof. Luca MESIN

Ing. Piero POLICASTRO

Candidate

Francesco GARDINI

21 Luglio 2023

POLITECNICO DI TORINO

Master degree course in Biomedical Engineering

Master Degree Thesis

Ultrasounds scans of Inferior Vena Cava in pneumological patients



Supervisors

Prof. Luca MESIN

Ing. Piero POLICASTRO

Candidate

Francesco GARDINI

21 Luglio 2023

Summary

Pulmonary diseases compromise the lungs function with an impairment of the gas exchange and an alteration of the respiratory mechanic. They are the third leading cause of death after cardiac and neoplastic ones and they have a strongly negative impact on the lifestyle and life expectancy.

Inferior vena cava (IVC) ultrasonography (US) can be important in clinical practice to evaluate patients with lungs disorders because IVC reflects changes of intrathoracic and abdominal pressure and its pulsatility is related to volume status and right atrial pressure.

The measures of the diameter of the vein are used to calculate three pulsatility indices: the caval index (CI), the respiratory caval index (RCI) and the cardiac caval index (CCI). However, this estimation is not reliable due to the movements of the IVC during respiration. In order to obtain a more stable measurement of the IVC pulsatility, a new software developed by VIPER srl was employed. It allows to track the edges of the vein and consequently to obtain a reliable measure of different diameters necessary to determine the pulsatility.

The aim of this study was to investigate the correlation between CI, CCI and RCI and the category of pulmonary disease in order to find differences between obstructive and restrictive pulmonary disease. For this purpose, several US scans, of both patients with lung disease and healthy subjects, were processed with the software mentioned above both in longitudinal and transversal view and a statistical analysis was conducted. A total of 29 patients was considered, 5 with an obstructive disease, 5 with a restrictive disease and 19 as control group. The median of CCI in longitudinal view was 0.12, 0.13 and 0.15 respectively for restrictive diseases, obstructive diseases and the control group. The median value of RCI was 0.1, 0.2 and 0.18 and that of CI was 0.2, 0.34 and 0.31.

In transversal view the median of CCI was 0.19, 0.21 and 0.16 respectively for restrictive diseases, obstructive diseases and the control group. The median value of RCI 0.18, 0.31 and 0.17 and that of CI was 0.37, 0.51 and 0.34.

Wilcoxon rank sum test was conducted in order to evaluate the presence of statistically significant differences between the three classes: no difference was found.

Moreover, a lumped-parameters model of the cardiovascular system was implemented in MATLAB to better understand the influence of the different variables

on the value of the most important pressures and volumes, both in physiological and pathological conditions. It is an innovative model based on the integration of different systems of ordinary differential equations that were found in literature; moreover, a description of the IVC was included. The model comprises two closed loops to describe the systemic and the pulmonary circulations and a time-varying elastance simulating the four cardiac chambers with their valves. Model's parameters were chosen to replicate both physiological conditions and the investigated pathologies. It can be used also to simulate heart failure and pulmonary hypertension that can be present in patients with advanced pulmonary diseases.

Acknowledgements

Vorrei ringraziare, innanzitutto, la mia famiglia per avermi incondizionatamente supportato in questo percorso a tratti travagliato ma estremamente entusiasmante. Ci terrei, inoltre, a ringraziare il Prof. Luca Mesin e l'Ing. Piero Policastro per avermi guidato e aiutato nel mio percorso di tesi. Vorrei, infine, ringraziare i miei amici per aver condiviso con me i momenti di gioia e per esserci sempre stati in quelli difficili.

Contents

Contents	5
List of Tables	7
List of Figures	8
1 Introduction	10
1.1 Anatomy and physiology of the inferior vena cava (IVC)	10
1.1.1 Anatomy of IVC	10
1.1.2 Mechanical behaviour of IVC during respiration	10
1.2 Fluid therapy	11
1.2.1 Volume status and fluid therapy in heart failure (HF)	11
1.2.2 Volume status and fluid therapy in patients undergoing dialysis	12
1.2.3 Volume status and fluid therapy in critically ill patients	13
1.3 Ecography	14
1.3.1 Physical principles of ultrasounds (US)	14
1.3.2 Echo-pulse technique	18
1.3.3 Doppler flowmetry	21
1.4 Heart Failure	25
1.4.1 Factors that influence the cardiac output	25
1.4.2 Symptoms and classification of HF	27
1.4.3 Pathophysiology	27
1.4.4 Compensatory mechanisms	29
1.4.5 Diagnosis and treatment	30
1.4.6 Acute heart failure (AHF)	31
1.4.7 Importance of RAP in the management of HF	32
1.5 IVC Ecography	34
1.5.1 Pulsatility Indices	34
1.5.2 Use of IVC ecography in the clinical practice	35
1.5.3 Limitations of IVC ecography	36
1.6 The Respiratory System	36
1.6.1 Anatomy of the respiratory system	36

1.6.2	Respiratory mechanics	37
1.7	Pulmonary diseases	40
1.7.1	Obstructive pulmonary diseases	40
1.7.2	Restrictive pulmonary diseases	40
1.7.3	Diagnostic Instrumentation	41
1.7.4	Restrictive pulmonary diseases vs Obstructive pulmonary dis- eases	43
1.8	VIPER Software	44
1.8.1	Longitudinal view	44
1.8.2	Transverse view	45
1.8.3	Estimation of CI,CCI and RCI	45
2	Statistical Analysis of caval indices in pneumological patients	47
2.1	Statistical Sample	47
2.2	IVC ultrasounds	47
2.3	Methods used for the statistical analysis	48
2.3.1	Boxplot	48
2.3.2	Wilcoxon Tests and Bland-Altman Plot	48
2.4	Results	51
2.5	Discussion	56
3	Cardiovascular System Model	58
3.1	Introduction to mechanics of the cardiac cycle	58
3.1.1	The Wiggers Plot	60
3.1.2	Pressure-Volume Loop (PV Loop)	60
3.2	Lumped parameters models	60
3.2.1	Analogy between cardiovascular system and electrical circuits	62
3.3	Method	64
3.3.1	Equations for the vascular compartments	64
3.3.2	Equations for the hearth	66
3.3.3	Implementation of Ursino Model	71
3.3.4	Implementation of atrial time-varying elastance and IVC de- scription	72
3.3.5	Modelling of the IVC respirophasic variations	74
3.4	Results	76
4	Conclusions	86
	Bibliography	88

List of Tables

1.1	Density, propagation velocity, acoustic impedance and attenuation of some tissues of interest. [24]	15
1.2	Attenuation of some tissues of interest. [24]	17
1.3	NYHA classification of different classes of HF. [36]	28
1.4	ACC/AHA classification of different stages of HF. [36]	28
2.1	Standard deviation (Std), kurtosis (Kur), skewness (Skw) and median (Med) for the three diameter components in longitudinal view	49
2.2	Standard deviation (Std), kurtosis (Kur), skewness (Skw) and median (Med) for the three diameter components in transversal view	50
2.3	Median value of caval indices	52
2.4	Median value of mean diameter	53
2.5	p-value of Wilcoxon rank sum test	54
3.1	Resistances, compliances and inertances of vascular compartments	71
3.2	Unstressed volumes of vascular compartments	72
3.3	Heart parameters	72
3.4	Resistances, compliances and inertances of vascular compartments before and after the tuning of parameters	73
3.5	Heart parameters for the atrial contractility and IVC model	74
3.6	Resistances, compliances and inertances of vascular compartments before and after the tuning of parameters	76
3.7	Values of pressures and volumes using Ursino Model.	78
3.8	Values of pressures and volumes using atrial contractility and IVC model.	79
3.9	Values of pressures and volumes using IVC respirophasic variations model.	82

List of Figures

1.1	Graphical representation of Snell's law.	16
1.2	Block diagram of an echo-pulse device. [24]	19
1.3	Scheme of two probe types: (a) linear probe, (b) sectorial scanning probe.	20
1.4	Example scheme of the PSD of the Doppler signal generated by 4 erythrocytes	22
1.5	Example scheme of the emission of two successive US packages	23
1.6	The Frank-Starling curve	29
2.1	Distribution of caval indices in longitudinal view.	51
2.2	Distribution of caval indices in transversal view.	52
2.3	Distribution of the mean diameter in longitudinal view.	53
2.4	Distribution of the mean diameter in transversal view.	53
2.5	Bland-Altman Plot for the comparison between the longitudinal and the transversal view for CCI.	55
2.6	Bland-Altman Plot for the comparison between the longitudinal and the transversal view for CI.	55
2.7	Bland-Altman Plot for the comparison between the longitudinal and the transversal view for RCI.	56
3.1	Stylized version of a P-V Loop [5].	61
3.2	Hydraulic circuit diagram; the red parts are those modified or added respect to Ursino model.	70
3.3	Wiggers Plot for the left heart.	78
3.4	Wiggers Plot for the right heart.	79
3.5	Wiggers Plot for the left heart - Atrial contractility and IVC model.	80
3.6	Wiggers Plot for the right heart - Atrial contractility and IVC model.	80
3.7	Comparison between the left atrial pressure trace obtained using Ursino model and that obtained after the implementation of the time-varying elastance model for the left atrium.	81
3.8	Comparison between the right atrial pressure trace obtained using Ursino model and that obtained after the implementation of the time-varying elastance model for the right atrium.	81
3.9	Wiggers Plot for the left heart - IVC respirophasic variations model.	82

3.10	Wiggers Plot for the right heart - IVC respirophasic variations model.	83
3.11	Comparison between the right atrial pressure traces with or without the influence of the respiration on IVC.	83
3.12	Volume and diameter of abdominal and thoracic IVC sections. Red and green dots indicate respectively maximums and minimums used for calculating CI	84
3.13	Comparison between IVC abdominal and thoracic volume.	84
3.14	Simulations of the influence of the two types of pulmonary diseases on IVC: A) Normal (thoracic) breathing, B) Restrictive disease, C) Obstructive disease.	85

Chapter 1

Introduction

1.1 Anatomy and physiology of the inferior vena cava (IVC)

1.1.1 Anatomy of IVC

The inferior vena cava (IVC) is a large vessel located at the posterior abdominal wall on the right side of the aorta, it has the largest diameter of the venous system. IVC originates from the confluence of the right and the left common iliac veins that usually takes place at the L5 vertebral level.[59]

It is the most important conduit for the transport of the deoxygenated blood from the abdomen, pelvis and limbs to the right atrium [56]. After ascending the abdomen and entering the thorax through the inferior vena caval foramen of the diaphragm, IVC reaches the the posterior inferior aspect of the right atrium.

1.1.2 Mechanical behaviour of IVC during respiration

Unlike many other veins, the IVC has not one-way valves to guarantee the forward flux of blood to the right atrium. The contraction of diaphragm and external intercostate muscles creates a negative pressure gradient that pulls blood toward the right heart.

As other veins and arteries, the IVC changes its shape and volume in response to the change in transmural pressure (p_{tm}), the difference between internal pressure (p_{int}) and external pressure (p_{ext}) according to its compliance.

$$p_{tm} = p_{int} - p_{ext}$$

The compliance is defined as the variation of volume determined by a certain variation of pressure. In general, the compliance is not constant: the greater the mean pressure, the smaller the variation of volume produced by a change of pressure.

$$C = \frac{\Delta V}{\Delta P_{tm}}$$

Transmural pressure varies following changes of internal pressure, that depends on intra-thoracic pressure, and those of external pressure which increase after the contraction of diaphragm [22]. For this reason, during the inspiration the size of IVC decrease: the intra-thoracic pressure is reduced and at the same time the contraction of the diaphragm produces an increase of the external pressure. The decreased intra-thoracic pressure causes a blood drainage from the abdominal IVC reflected in a increased venous return [9]. Opposite, during exhalation the intra-thoracic pressure increases and the abdominal one decrease, this is reflected in higher blood flow from lower limbs to abdominal IVC and a reduced venous return. Different studies have shown that the respiration pattern strongly influences the amount of the reduction in IVC size. In particular, the diaphragmatic breathing induces several occlusion of the lumen of IVC [22].

1.2 Fluid therapy

The intravascular volume status, which could be defined as the volume of blood in the circulatory system, is a very important cardiovascular parameter related to the cardiac preload, the stretching of the cardiomyocytes before the systole. It influences the force of contraction of the cardiac muscle and consequently the cardiac output and the arterial blood pressure.

The assessment of the intravascular volume status is essential for the treatment and the management of several pathological condition like heart failure (HF), diseases that require dialysis and severe sepsis, in order to establish the correct fluid therapy. Actually the most accurate and reliable way to asses volume status of a patient is to measure the right atrial pressure (RAP), which normally is between 2 and 6 mmHg, or the pulmonary capillary wedge pressure (PCWP), which usually vary between 3 and 8 mmHg [15], by right heart catheterization (RHC). It is an invasive procedure and not routinely executed, therefore, it is not suitable for the follow-up of the patient [8].

1.2.1 Volume status and fluid therapy in heart failure (HF)

Congestion in hearth failure consists of a fluid accumulation in the intravascular compartment and in the interstitial space caused by an increased cardiac filling pressure due to a dysfunction in the sodium and water retention process.

Intravascular congestion is the result of a combination of haemodynamic and neurohormonal factors that leads to a retention of sodium and water by kidneys. The increased hydrostatic pressure in the vessels produce can tissue congestion, indeed, the unbalance between the hydrostatic pressure and the oncotic pressure in the interstitium can promote the development of tissue oedema [15].

Congestion is the main cause of hospitalization in patients with decompensated hearth failure, in Europe 83 % of patients hospitalized with HF shows clinical signs of congestion [15]. Moreover, patients with residual congestion after 7 days of hospitalization have a twofold increase in 180-day mortality and an almost risk twofold risk of rehospitalization for HF [15]. Intravascular congestion can be asses in different ways, using clinical signs like the distension of the jugular vein, the orthopnea or the third sound, or with the analysis of some biomarkers such as natriuretic peptides (NT-proBNP) and the haemoconcentration. In clinical approach also imaging method are often employed to establish the volume status of a patient, the most common are the ultrasonography of IVC, jugular vein or renal venous district.

The cornerstone of fluid therapy for the decongestion in case of hearth failure is the administration of loop diuretics. They block the reabsorption of sodium and consequently they promote an increased excretion of sodium and urine output. Thanks to the mechanism of natriuresis fluid loss is achieved because the free water passively follows the excreted ions.

Acqueresis is another way to induce fluid loss, it consists in the direct excretion of free water, through the translocation of fluid from the interstitium to the intravascular space. For this reason, drugs that promote acqueresis are more suitable for the treatment of tissue congestion. [15]

1.2.2 Volume status and fluid therapy in patients undergoing dialysis

As mentioned before, the volume status is a critical parameter in patients undergoing dialysis, the management of intravascular volume is one of the most challenging aspects in this kind of therapy. Indeed, a chronically hypervolemia leads to hypertension, hearth disease and tissue oedema, at the same time hypovolemia during dialysis causes nausea, cramps, vomiting and a general decreased patient satisfaction. Hypovolemia is most frequent complications of hemodialysis, its onset varies from 10% to 30% depending on the population studied [13].

Clinically assessed dry weights, the lowest weight post-dialysis at which the most of exceed fluids have been removed, is the most common way to establish the volume status of a patient. Despite its widely diffusion, it is an unreliable and poor predictive measure of the volume status [13]. Actually, ultrasography of IVC is one of the most promising tool in order to improve the reliability in the volume assessment in patients undergoing dialysis.

1.2.3 Volume status and fluid therapy in critically ill patients

Assessment of volume status as well as the response to a fluid challenge in terms of an increased cardiac output is an important task in the care of critically ill patients. Several approaches that provide an aggressive fluid resuscitation are able to reduce organ failure and mortality in patients with severe sepsis or sepsis shock. On the other hand, some studies on critically ill patients have shown that a large fluid overload and a net positive fluid balance are connected to a higher risk in the onset of complications and an increased mortality [34].

The most important reason to give a patient a fluid challenge is to increase the stroke volume [34], the volume of blood ejected by a ventricle for each systole, in order to improve organ perfusion.

For these reasons, the assessment of the volume status in critically ill patients and their response to a fluid challenge is crucial in order to establish and to modulate the appropriate fluid therapy.

1.3 Ecography

Ecography is widely used in medicine for several reasons [24]:

- It is safe for the patient: ionising radiation aren't necessary for this imaging technique, for this reason it suitable for long exams and for follow-up protocols that require several repetition of the examination at short interval time. It is also possible using it on high-risk patients like pregnant women.
- It is the exam with the highest temporal resolution coupled to a good spatial resolution. It is possible to monitor phenomena that change very quickly, like the opening and the closure of an heart valve.
- It is based on the physical principles of reflection and diffusion so it can provide different and complementary information compared to other exams.

Actually, ecography is employed in many areas of medicine to study different organs and them structural alterations that often are a pathological sign. There are many kinds of US devices that can be used in different situation, from portable ultrasound scanners that can be connected to a PC or smartphone to complex workstations.

1.3.1 Physical principles of ultrasounds (US)

US are elastic waves that produce compression and rarefaction, when the wave is positive or negative respectively, of the medium they pass through. The molecules that constitute a tissue move in harmonic motion, swinging around the equilibrium position, when perturbed by an ultrasound wave. US are sounds whose frequency exceeds that audible to human ear ($f > 20$ KHz), in medicine the most common US devices employ frequencies in the order of 1-10 MHz. [24]

The following relation correlates the propagation velocity (v) of a generic wave to its frequency (f) and wavelength (λ):

$$v = \lambda f \tag{1.1}$$

The US velocity in the biological tissue is almost constant with the exception of lungs and bone, conventionally a mean value of 1540 m/s is used. [24]

The medium acoustic impedance (Z) is an other important medium property on which US imaging techniques are based:

$$Z = \rho v \tag{1.2}$$

where ρ is the density of the medium and v the propagation velocity.

Tissue	ρ [Kg m ⁻³]	c [m s ⁻¹]	Z [Kg m ⁻² s ⁻¹]
Air	1.3	330	429
Water	1000	1480	1.5x10 ⁻⁶
Fat	900	1450	1.3x10 ⁻⁶
Muscle	1080	1585	1.7x10 ⁻⁶
Lung	220	900	0.2x10 ⁻⁶
Blood	1030	1570	1.6x10 ⁻⁶
Bone	1850	4000	7.4x10 ⁻⁶

Table 1.1. Density, propagation velocity, acoustic impedance and attenuation of some tissues of interest. [24]

US are generated exploiting the piezoelectric effect: some materials are able to generate a potential difference ΔV when submitted to a pressure (Direct piezoelectric effect) and to deform themselves when a tension is applied (Inverse piezoelectric effect). Both direct and inverse piezoelectric effect are employed in order to detect and to generate US respectively.

Actually, most of transducers are made of PZT (lead zirconium titanate). Considering that the velocity of US in PZT is about 4000 m/s and that resonance occurs for a thickness (h) equal to the half of the wavelength, it is simple to derive that for a frequency of 5 MHz:

$$h = \frac{\lambda}{2} = \frac{v}{2f} = \frac{4 \cdot 10^6}{2 \cdot 5 \cdot 10^6} = 0.4mm \quad (1.3)$$

In general, the frequency (MHz) of the US generated using piezoelectric effect is: $f = \frac{2}{h}$, with h expressed in mm.

In an homogeneous medium US propagate along a straight line, the transducer is lean on layer of a special gel that avoid the air interposition between the probe and the skin. When a wave meets an interface separating two mediums with different acoustic impedance, one part of the energy is transmitted and another is reflected or diffused.

The Snell's Law describe this phenomenon:

$$\frac{\sin \theta_i}{\sin \theta_t} = \frac{v_1}{v_2} \quad (1.4)$$

where θ_i is the angle of the incident wave, θ_t the one of the transmitted wave and v_1 , v_2 are the velocities in the medium 1 and 2 respectively (figure 1.1). If the velocities are equal the US wave continues without deviation, similarly if the acoustic impedance is the same in the two mediums all the energy of the wave is transmitted and there is not reflection. As said before, if the acoustic impedance

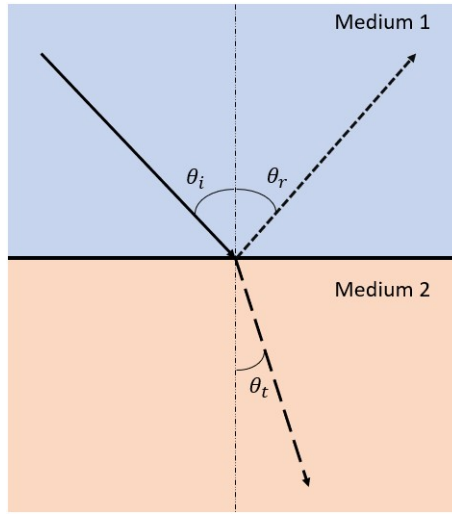


Figure 1.1. Graphical representation of Snell's law.

of the mediums are different part of the energy is reflected with angle equal to the one of incidence. The reflection coefficient (R) describe the fraction of the reflected energy and it is given by the following formula:

$$R = \left(\frac{Z_1 \cos \theta_t - Z_2 \cos \theta_i}{Z_1 \cos \theta_t + Z_2 \cos \theta_i} \right)^2 \quad (1.5)$$

In the ultrasonography approach angles are not considered and (1.5) become [24]:

$$R = \left(\frac{Z_1 - Z_2}{Z_1 + Z_2} \right)^2 \quad (1.6)$$

The transmission coefficient (T) is defined as $T = 1 - R$ with $0 \leq R \leq 1$. If the acoustic impedance of two tissues is the same or their difference is very small R is close to 0, the problem of detectability arises. It is impossible to distinguish the two different tissues, indeed, US imaging is able to show only difference between different tissues and it doesn't give any information about the single tissue. As well as, if $Z_1 \gg Z_2$ or $Z_2 \gg Z_1$ like in the interface muscle-bone or for the presence of air, R is almost equal to 1 hence all the energy is reflected, producing a white image.

The intensity of a US wave is attenuated by the tissue passing through, energy is partly absorbed or diffused (if dimension of the particles is comparable with that of wavelength) and it decreases following the equation:

$$A(z) = A_0 e^{-\alpha z} \quad (1.7)$$

where A_0 is the initial wave intensity and α is the attenuation coefficient. The intensity decreases exponentially in function of the space travelled.

Tissue	Attenuation ($dBcm^{-1}MHz^{-1}$)
Air	>10
Water	0.002
Muscle	1.5
Fat	0.6
Lung	30
Blood	0.18
Bone	8

Table 1.2. Attenuation of some tissues of interest. [24]

Attenuation depends on the nature of the tissue, as shown in the table lungs, air and bone strongly attenuate US, for this reason these mediums act as barriers for the propagation of US.

Attenuation is also related to frequency, in particular the higher the frequency the greater the attenuation. In medicine it is necessary being able to discriminate elements in the range of millimetres or even smaller, remembering equation (1.1) it is clear that spatial resolution (depending on wavelength) increases for higher frequencies. A compromise between the spatial resolution and the attenuation, hence the maximum attainable depth, is required.

1.3.2 Echo-pulse technique

Modern ecography systems are made of a probe that contains several PZT crystals which are piloted by a tension generator, an amplification system and device to view the image. The tension generator has a central role indeed it has to be able to generate the impulse with the correct amplitude and frequency. US imaging is based on the principle of reflection, emitting US impulses on a line and listening to the returning echo it is possible to establish the position of the interface of two tissues with different acoustic impedance. The distance (d) of the interface, calculated on the basis of flight time Δt (the time employed by the US wave to reach the interface and to come back to the probe), is given by:

$$d = \frac{1}{2}c\Delta t \quad (1.8)$$

where c is the velocity in the mean biological tissue (1540 m/s).

Usually the transducers are excited not with a single wave but with a package of waves (made of at least of 2 or 3 waves), after that they commute in the reception mode in order to pick up the returning echo of the package just emitted. This process is controlled by an electronic circuit that appropriately pilots the tension generator.

The returning signal is then amplified through the Time Gain Compensation system (TGC). Indeed, amplitude of the the returning echo is influenced not only by the difference in acoustic impedance at the tissue interface but also from the depth that determines the attenuation of the signal. For this reason, TGC is a logarithmic amplifier that use the flight to proportionally amplify the returning echo, in this way a superficial echo will be amplified less than a deeper signal. After the TGC the amplitude of the returning signal will be function of the difference in acoustic impedance of the tissues (R), which corresponds on the grey level of the final image, while thanks to the flight time it will be possible the establish the position of the interface (figure 1.2).

The spatial resolution depends on the way with which the transducer is excited, in particular three values spatial resolution are defined, the axial spatial resolution along the line of propagation, the later one perpendicular to the line of propagation and the one of elevation. As said before, the spatial resolution is correlated to the length of the wave package, to shortening it is possible to increase the frequency of the the wave inside the package. However, higher frequency waves are less penetrating. Generally, the axial spatial resolution is 2-3 times the wavelength (λ) while the lateral one is 2 or 10 times λ depending on the beam focusing.

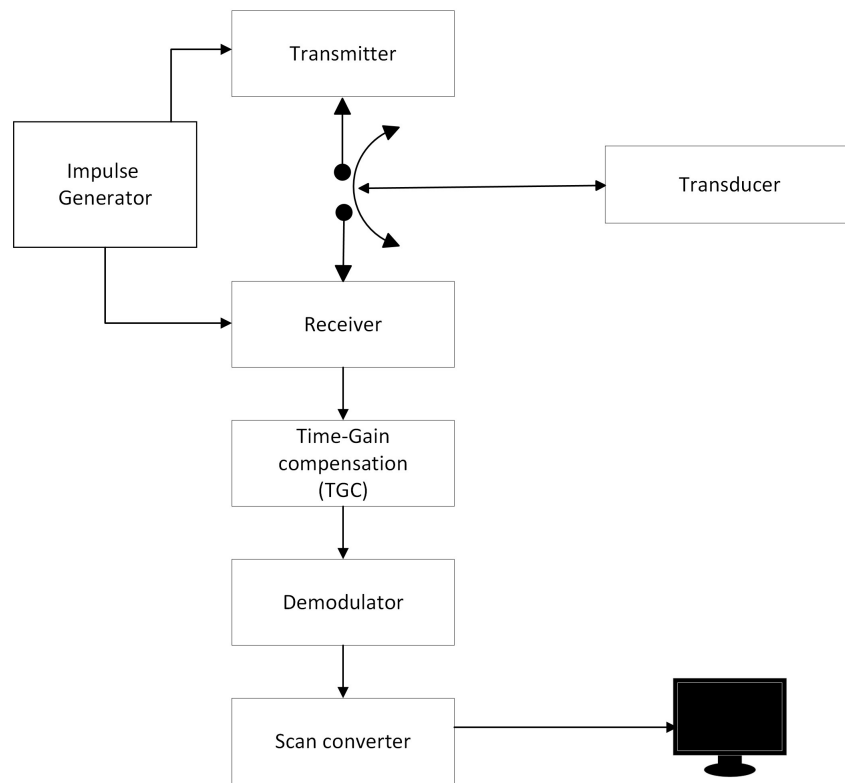


Figure 1.2. Block diagram of an echo-pulse device. [24]

Scanning techniques

The scanning of organs of interest can be achieved using a single transducer or with a multiple transducer. In the first case the single element can be pilot with a manual movement or with an automated device. It's a rotating probe constituted of several transducers, the active element is the one facing the surface to be explored. Currently it's an obsolete system and it is no longer used.

The most of the probes used in medicine are made of an array of transducers, they are activated in a specific order using an electronic circuit. The different crystals are activated in specific sequence through which it is possible to change the beam shape. In the linear probes, used especially in obstetrics, all the element are parallel activated while in the sectorial scanning probe the beam diverge in order to explore relatively large areas (figure 1.3). The phased array technique allows to focus the beam in specific direction and depth or to deflect the beam, this is made possible by piloting the time of emission of the different impulses.

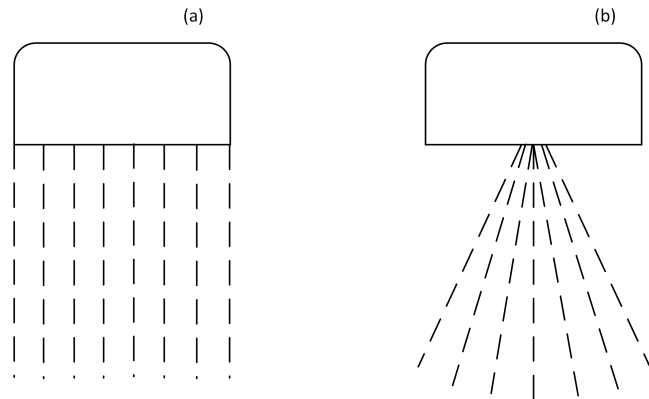


Figure 1.3. Scheme of two probe types: (a) linear probe, (b) sectorial scanning probe.

Visualization modes

There are different ways to visualize the information of returning echo signal:

- A-mode (amplitude): a single transducer is used and the signal in function of time is showed on the display. The time corresponds to the depth while the amplitude is related to intensity of the reflection. It is used for very simple exams or conversely for advance analysis in which the waveform is studied in order to understand the medium crossed.
- B-mode (Brightness): the echo signal module the amplitude of the Z-axis of the display, in other world the pixel brightness. Greater the amplitude of the signal, greater the the brightness; Instead, the flight time determines the position.
- M-mode (Time motion): It is obtained by placing several B-Mode sequences at opportune moments of time, conventionally x-axis represents the time while y-axis the displacement from the probe. Using this modality it is possible to follow the movement of some elements of interest like an hearth valve or a ventricle wall. For this reason it is widely used in cardiology.

1.3.3 Doppler flowmetry

US allow to measure the mean velocity or to show the velocity profile inside a vessel using the Doppler effect. Indeed, the corpuscular part of the blood having a smaller diameter than the US wavelength acts as non-specular reflectors that diffuse the energy in all directions. For the Doppler effect they cause a variation (δf) of the US beam frequency (f_0) given by the following formula:

$$\delta f = f_D - f_0 = \frac{2f_0 v \cos \theta}{c} \quad (1.9)$$

where f_D is the frequency modified by the Doppler effect, v the blood velocity inside the vessel, c the US velocity and θ the angle between the propagation direction of the US beam and the longitudinal axis of the vessel. As in the case of the echo-pulse technique the frequency of the transducer determines the maximum depth, as well as the frequency of repetition of the impulses that is strongly related to the time employed to reach the established depth and to come back to the receiver. The angle θ is one of the most influential variables in this kind of examination, if the US beam was perpendicular to the vessel ($\theta = 90^\circ$) the Doppler signal would be null, while for $\theta = 0^\circ$ (US beam parallel to the vessel) it would be maximum. The last case is almost impossible to occur, in practice the most accurate results are obtained with an angle between 40° and 60° because in this range of values the cosine function is almost linear.

Information provided by Doppler signal

The frequency of the returning echo is proportional to the velocity of erythrocytes, the power spectral density (PSD) of the signal reflects the velocity distribution inside the vessel. Each erythrocyte with a certain velocity generate an echo with a corresponding frequency f_D , greater the number of erythrocytes higher the amplitude of the PSD of the Doppler signal for that specific frequency. Thus, the area of the the spectrum gives an estimation of total number of erythrocytes, it is possible to measure the flow. The bandwidth as well as the shape of the signal is related to the speed profile, indeed, if all erythrocytes had the same velocity there would be only a frequency in the PSD while if all velocities had the same probability to occur the spectrum would be flat.

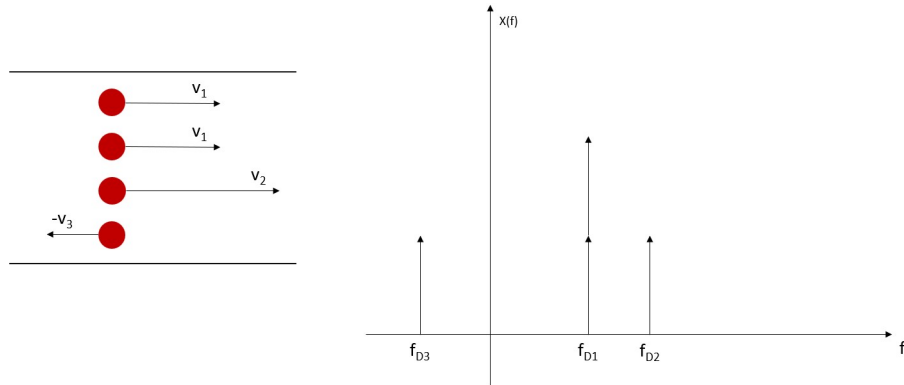


Figure 1.4. Example scheme of the PSD of the Doppler signal generated by 4 erythrocytes

Pulsed Doppler

The probe of pulsed Doppler devices acts both as transmitter and receiver. Measuring the returning time of the echo it is possible to map the entire volume of the vessel and thus to show the velocities profile. As said before the shape of the spectrum reflects the distribution of velocities, in particular, if the mean and the maximum velocities are similar almost all erythrocytes have the same velocity and the spectrum is very narrow. Conversely, in case of parabolic profile flow the mean and maximum velocities are different.

Continues wave Doppler

In the continues wave Doppler devices the probe is made of two crystals, one is the emitter and the other is the receiver, this makes it possible to use higher frequency in order to detect higher velocities, particularly useful in pathological cases. However, the maximum reachable depth is reduced and it is not possible the generate the profile velocities. Indeed, using different crystal it is impossible to measure the returning time of echos and relate them to a corresponding frequency.

Pulse Repetition Frequency (PRF)

The pulse repetition frequency is the frequency with whom the US packages are emitted by the probe, in flowmetry is particularly important because it indicates the time interval between two successive packages (Pulse Repetition Period, PRP) (figure 1.5).

$$PRF = \frac{1}{PRP} \quad (1.10)$$

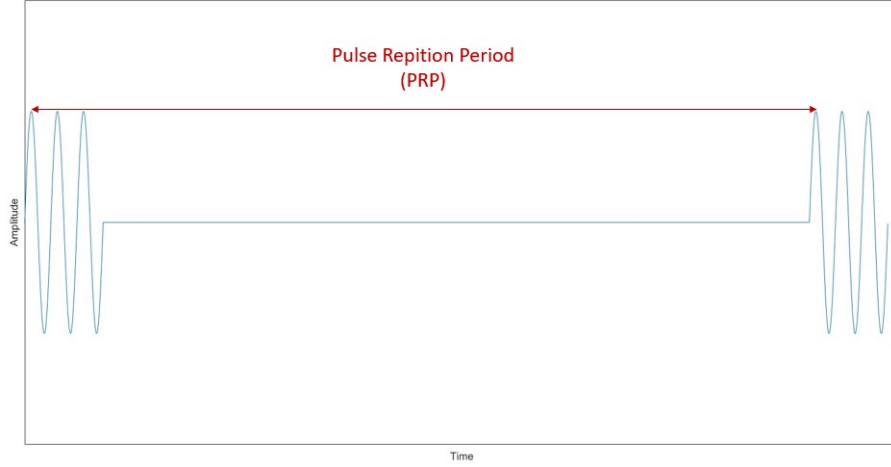


Figure 1.5. Example scheme of the emission of two successive US packages

The echo of a US package must return to the probe before the next package is emitted, hence the PRF determines the maximum reachable depth:

$$d_{max} = \frac{c}{2PRF} \quad (1.11)$$

According to the equation (1.9) the maximum velocity (v_{max}) corresponds on the maximum Doppler frequency (f_d), the Nyquist theorem says that the sample frequency must be at least two times the maximum frequency to avoid aliasing:

$$PRF \geq 2f_{Dmax} \quad (1.12)$$

Therefore, PRF determines the maximum velocity detectable:

$$v_{max} = \frac{PRFc}{4f_0 \cos \theta} \quad (1.13)$$

Hence, continuous wave doppler device are more suitable to measure high velocities at significant depths.

Power Doppler and color Doppler

This two modalities typical of the US imaging add a color coding to the morphological image obtained in B-mode.

In the color Doppler method the color coding serves to identify and to monitor the direction of the blood stream:

- Blue color corresponds on a a flux concord to the direction of propagation of the US beam
- Red color is associated to retrograde flux, in the opposite direction respect to direction of propagation of the US Beam

The luminosity of the color is related to the module of the velocity.

In the power Doppler the color is proportional to the intensity of the spectrum in that point, the object of interest in this case is the number of erythrocytes instead of the velocity. It is calculated computing the the integral of the spectrum. It is particularly useful to examine weak flows like those in cerebral arteries.

Ecography with medium contrast

A medium contrast can be used in order to emphasise vascular districts that would be difficult to visualize with the US imaging methods described in the previous sections. The idea behind this technique is to make echogenic the blood increasing the difference in acoustic impedance with surrounding tissues. The medium contrast is injected and it is made of microbubbles of an heavy gas (usually SF_6 , sulphur hexafluoride) encapsulated in a lipid layer in order to improve their mechanical properties and to increase the permanent time inside the vessel. The echogenicity can increase 20-fold and the reflectivity is proportional to the volume of microbubbles injected. The resonance frequency of the microbubbles is in the range of frequency commonly used in the Doppler flowmetry. However two possible kinds of artifacts can be found using this method: color blooming and saturation. The first one is due to the rapid diffusion of the medium contrast and causes an intense colour of all the area of interest. it is possible to avoid waiting few minutes before starting the exam after the medium contrast was injected. The saturation consists in a false indication of increased velocity cause by the rupture of the single bubbles bigger than others.

1.4 Heart Failure

Heart failure (HF) is a complex pathology that in general causes a reduction of the the cardiac output (CO) which becomes insufficient to accommodate the metabolic or venous return requirements. HF is the consequence of a loss of critical quantity of myocardial cells caused by different pathologies. The most common are: ischemic heart disease, hypertension and diabetes. Other important causes, but less common, are cardiomyopathies, infections, toxins, valvular disease and arrhythmias. [36]

HF is a widespread pathology that affect about 1-2 % of the adult world population, and several reports show that it is rapidly expanding. Actually it is more common in the high-income country, probably due to the higher diffusion of hypertension, diabetes and coronary heart disease (CHD)[16]. A 2012 report estimates that the direct cost across the globe to manage patient affected by hearth failure is about \$65 billion per annum.[16]

1.4.1 Factors that influence the cardiac output

The cardiac output is the volume of blood ejected in 1 minute by each ventricle and it is equal to the product of the stroke volume (SV), the volume of blood ejected each systole by a ventricle, and the heart rate (HR) [57].

$$CO = SV \times HR \quad (1.14)$$

In normal condition considering an HR of 70 bpm and a SV of 70 mL, the CO is about $5 \frac{l}{min}$. [57]

The CO of the left and right ventricle correspond on the system blood flow and on the pulmonary circle blood flow, respectively. Over the long period they must be equal in order to avoid an accumulation of blood in the systemic circle, or vice-versa.

Knowing that CO depends only on two variables, controlling the factors that influence them it is possible to modular the CO.

The heart rate is mainly regulated by the autonomous nervous system that act on the conduction system and on the cardiac tissue. In particular, the pacemaker cells of the atrial sinus node (SA) that regulate the frequency generation of the action potential responsible of the myocardium contraction, receive afferents from both sympathetic and parasympathetic neurons. The activation of the former produces an increase of the frequency of the action potential causing an increase of the heart rate, vice-versa the action of the parasympathetic system produce a decrease of the hearth rate. Several hormones influence the heart rate, adrenalin is the most important of them. It is able to increase the frequency with which action potentials are generated in the SA node and thus the to increase the heart rate. Thyroid

hormones, insulin and glucagon are other important hormones that can modulate the heart rate acting primarily on the contraction force of myocardium.

The stroke volume is regulated mainly by three factors: contractility, the telediastolic volume (preload) and the afterload.

The term contractility describes the muscle's ability to generate force, it is primarily influenced by the autonomous nervous system, in particular the sympathetic nervous system. Indeed, neurons directly innervate muscle cells of atria and ventricles, their activation produces an increase of the contraction velocity and the force generated by myocardial cells. Hormones like insulin, glucagon and adrenalin also can rise the myocardial contractility.

An other factor that is strongly related to the ventricle's contraction force is the stretching of the myocardial cells when the ventricle is filled with blood. The Starling Law says that when the venous return changes, hearth automatically adapts the the outflow respect of the inflow. It is based on the Starling effect: higher the telediastolic volume (Volume of blood at the end of the diastole), greater the ventricle contraction force. This is due to the fact that the myocardial cells reach their maximum efficiency for a longer length than that at rest, thus an increase in the telediastolic volume leads the fibers to work closer and closer to their optimal length. The telediastolic volume is mainly determined by the telediastolic pressure, also known as preload, it establishes the myocardial tension before the contraction. Indeed, the pressure causes the expansion of ventricle walls that is filled with blood, a greater pressure corresponds on a higher volume at the end of ventricle diastole. In turn, the preload depends on other factors like the hearth rate, the atrial pressure that is determined by the venous return and the atrial contraction force. In particular, greater the central venous pressure (the pressure inside the large veins that bring blood back to the heart) higher the blood flow to the atria. This leads to an increase of the atrial pressure and consequently of the preload.

When the ventricle contracts during the systole it works against the arterial pressure, a rise in the latter tends to decrease the stroke volume. The arterial pressure sensed by ventricles after the beginning of the systole is known as afterload. Generally, higher mean arterial pressure, greater the afterload.

In this section the most important factor that influence the cardiac output have been individually analysed, however, they can change simultaneously and the effective regulation of the CO is the result of them combination.

1.4.2 Symptoms and classification of HF

The typical symptoms of heart failure are the consequences of the insufficient CO requested to accommodate metabolic activity and venous return. One of the final effects of HF is the rise of the left atrial pressure that produces an increase of the pressure in the pulmonary capillary bed. This in turn leads to the onset of dyspnea, cough and wheezing. Other common signs of HF are lower extremity edema and ascites due to the incapacity of the right heart to accommodate venous return. Generally, fatigue also during moderate physical activity is present in patients with HF, as well as palpitation caused by an increased heart rate.

Currently, HF is classified using two different classification systems: the first one was developed by the New York Heart Association (NYHA) and it classifies patients in 4 classes on the basis of the onset of fatigue for different intensities of physical activity and eventually at rest (table 1.3)[36]. The second one was designed by the American College of Cardiology (ACC) and the American Heart Association (AHA) and it emphasizes the evolution and the progression of the disease[36]. It classifies patients in 4 classes taking into account the importance of the risk factors and the structural prerequisites for the development of HF (table 1.4). In particular, this system is based on the assumption that an adequate intervention before the onset of the dysfunction can decrease the mortality associated to this pathology. Both methods are used to establish the correct therapy and in both the first and the second the mortality rises as classes progress.

1.4.3 Pathophysiology

First of all it is possible to distinguish the failure of the left ventricle (LV) or the right ventricle (RV). The left ventricular dysfunction can be divided in two categories on the basis of the ejection fraction (EF), the percentage of the end-diastolic volume ejected during the systole: if the EF is $< 40\%$ it will be a systolic dysfunction, caused by an impaired ventricular contraction and ejection. If EF is $> 40\%$ it will be a diastolic dysfunction due to the decoupled relaxation and ventricular filling.[36]

The most important cause in the onset of the LV systolic dysfunction is the loss of myocardial cells caused by ischemic disease and infarction; other leading factors are hypertension, volume overload due to valvular failure and arrhythmias. One of the ultimate of LV dysfunction is a global hypo-perfusion, in addition the reduced EF causes a rise of the end-systolic and end-diastolic volumes that produces an increase in the left atrial pressure leading to an increase of the pressure of the capillaries in the lungs. This elevated pressure causes the spill of fluid and thus pulmonary congestion. The symptoms of systolic and diastolic HF are the same and, as said before, they are the result of an elevated atrial pressure and pulmonary congestion.[36] The leading cause of right ventricular failure is LV dysfunction. Also in this case,

NYHA classification	
Class I	No symptoms with ordinary activity
Class II	Slight limitation of physical activity, comfortable at rest, but ordinary physical activity results in fatigue, palpitation, dyspnea, or angina
Class III	Marked limitation of physical activity, comfortable at rest, but less than ordinary physical activity results in fatigue, palpitation, dyspnea, or angina
Class IV	Unable to carry out any physical activity without discomfort Symptoms of cardiac insufficiency may be present even at rest

Table 1.3. NYHA classification of different classes of HF. [36]

ACC/AHA classification	
Stage A	Patient at high risk for developing HF with no structural disorder of the heart
Stage B	Patient with structural disorder of the heart without symptoms of HF
Stage C	Patient with past or current symptoms of HF associated with underlying structural heart disease
Stage D	Patient with end-stage disease who requires specialized treatment strategies

Table 1.4. ACC/AHA classification of different stages of HF. [36]

an increase of the right atrial pressure produce fluid congestion. In particular, the rise of the pressure in the inferior vena cava leads to a several clinical signs like

abdominal pain, hepatomegaly and peripheral edema.

1.4.4 Compensatory mechanisms

The cardiac output is strongly related to the mean arterial pressure (MAP), indeed, it can be defined as the product between the CO and the total peripheral resistance (TPR)[36] [57]. As said in previous section, a patient with HF shows a decreased that cause a fall of the MAP and consequently a general hypo-perfusion. The body try to compensate a change of the MAP using different mechanism, the most common are the Frank-Starling mechanism, neurohormonal activation and ventricular remodelling.

Frank-Starling mechanism

The Frank-Starling effect says that an increase of the preload produces a rise of the stroke volume, this mechanism is used in order to compensate a lowering of the MAP. In patient with HF initially this effect causes an increase of CO as expected, but with the progression of the disease next increments of preload do not corresponds on rise of the stroke volume. This situation is explained by the Frank-Starling curve: the curve tends to flatten out as preload increases, this is even more evident in patient with heart failure. At this point increments in preload lead to pulmonary congestion.

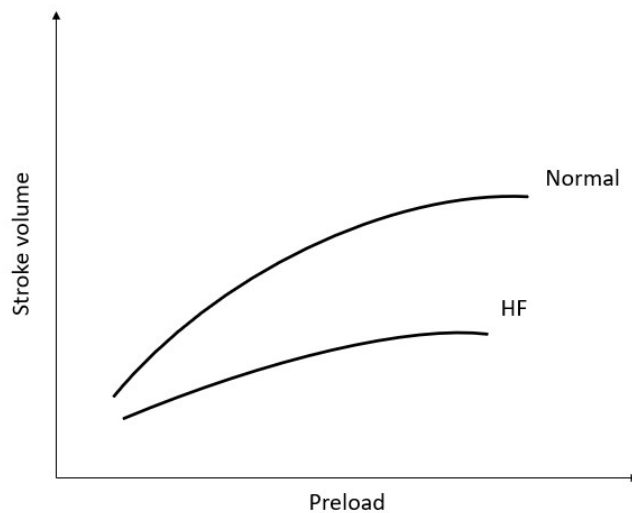


Figure 1.6. The Frank-Starling curve

Neurohormonal activation

Several hormones are able to regulate MAP acting primarily on the TPR, it is an important compensation during the first stages of HF. The lowering of the MAP typical of HF stimulate the sympathetic nervous system that promote the release of norepinephrine and epinephrine. This hormones act on the heart increasing the heart rate and the contractility, at the same time, on the vascular system causing vasoconstriction. This combined effect produce an increment of the MAP. The decreased MAP lead also to the activation of the renin-angiotensin-aldosterone system, it is a complex system of chain-reactions that involves different organs. In the end angiotensin II in addition to promote vasoconstriction, facilitates the excretion of aldosterone. The final result is the the sodium reabsorbtion and the release of norepinephrine and vasopressin that stimulate vasoconstriction. Vasopressin release is facilitated also by a negative feedback loop; the lowering of map is detected by baroreceptors that decrease their inhibitory effect on hypothalamus promoting vasopressin release. This is a very power full compensatory mechanism used to manage the physiological change of MAP, however its continuous activation in patient with HF on the long-term results in ventricular remodelling that can cause myocardial dysfunction [36].

Ventricular remodelling

Ventricular remodelling is complex and long process that consists in the change in shape, geometry and mass of the ventricle. It occurs when the ventricle is subjected to a large hemodynamic stress produced by an excessive preload and afterload for a long period of time. During ventricular remodelling the wall thickness and the overall mass of the ventricle increase, it is a progressive process that results harmful on the long term. The elavated dimension of the heart induces fibrosis of the tissue with the consequent apoptosis of a critical number of myocardial cells. Moreover, the dilated ventricle is less efficient at pumping blood resulting in a decreased CO. The progression of the disease leads to triggering of a vicious circle that produce a progressive ventricle dysfunction and death.

1.4.5 Diagnosis and treatment

The first phase of the diagnosis process aim to investigate the symptoms of the patient and to evaluate the clinical history, this can help to determine the causes of the heart failure. Electrocardiogram is one of the most use full exams to asses HF as well as echocardiography. The first one permits to evaluate the presence of infarct or ischemia, arrhythmias or conduction problems, the second is indispensable to show the geometry of the hearth chamber, to measure the mass, the ventricle ejection fraction and other important parameters to establish the the status of the

disease. An other important evaluation is the level of some biomarkers, like natriuretic peptides (BNP, NT-proBNP), in order to identify the not only HF but also the eventually dysfunction of other organs like liver and kidneys.[39]

In the last 30 years several studies have been conducted in these area in order to understand the underlying physiological causes of HF and the most efficient therapy to improve the prognosis and the quality of life of the patient. Currently there are international guidelines that define the different kind of hearth failure, the diagnosis methods and the suggested therapy and clinical approach for each one. The most common and widespread therapies include pharmacological treatment, eventually the implantation of medical device like ICDs, pacemaker or left ventricular assist device (LAVD) and the lifestyle modification.

Generally, the pharmacological therapy aim to reduce the detrimental effect of the over-activation of the compensatory mechanisms described in the previous section. It aim to modulate the activation of the renin-angiotensin-aldosterone system (RAAS) and the sympathetic nervous system using angiotensin-converting enzyme inhibitors (ACE-I) or angiotensin receptor-neprilysin inhibitor (ARNI), beta-blocker and mineralocorticoid receptor antagonist (MRA). With the progression of the disease the ultimate treatment is still the heart transplantation[39].

1.4.6 Acute heart failure (AHF)

Acute heart failure is a complex and heterogeneous syndrome characterized by a new onset or a worsening heart failure requiring an urgent treatment and an unexpected hospitalization . Heart dysfunction, typical of HF, is a necessary condition that is often coupled to a systemic and pulmonary vascular dysfunction which cause a severe hemodynamic stress. AHF is not only associated to heart, it involves other organs like kidneys and liver. AHF is often triggered by ischemia, hypertension, arrhythmias, non cardiac comorbidities, and administered drugs.[52]

As said before, AHF causes an elevated hemodynamic response that is reflected in reduced cardiac output, increased filling pressure and afterload.

The different causes contributing to the onset of AHF are reflected in the wide spectrum of clinical manifestations, those of congestion due to an elevated ventricular filling pressure are one of the most common. Thus, physical examinations and laboratory tests are fundamental in order to establish the causes triggering AHF for therapeutic decision-making. Parallel to the diagnostic process to asses HF, a careful evaluation of the patient clinical profile is necessary to identify eventually life-threatening conditions[52].

Following the European Society of Cardiology guidelines, there are four major clinical presentation of AHF [39]:

- Decompensated Chronic Heart failure (ADHF): this condition is characterized by the worsening of signs and symptoms typical of chronic HF. Pulmonary or systemic congestion and peripheral oedema are often present in patient with ADHF. Sometimes hypoperfusion is encountered.
- Pulmonary oedema: the onset of signs and symptoms is rapid and the patient shows tachypnea, orthopnea and pulmonary congestion.
- Isolated right ventricular failure: it is associated with an elevated ventricular and atrial pressure and systemic congestion but with a low left ventricular pressure and the absence of pulmonary congestion.
- Cardiogenic shock: it is characterized by a severe peripheral hypoperfusion caused by an inadequate cardiac output, it can compromise vital organ leading to death.

1.4.7 Importance of RAP in the management of HF

Right atrial pressure (RAP) is related to the venous return that is in turn determined by the central venous pressure (CVP), the greater the volume of blood the greater the pressure. It is a key parameter in the assessment and management of HF, especially to evaluate the patient volume status coupled with the pulmonary capillary wedge pressure (PCWP) that is an indirect measure of the left atrial pressure [15].

Relation between LV dysfunction and RV dysfunction

Left ventricular dysfunction results in pulmonary hypertension (PH) defined by a mean pulmonary artery pressure (PAP) ≥ 25 mmHg [54]. Change in heart chamber shape and eventually mitral regurgitation (MR) contribute to the rise of left-sided filling pressure leading to an increase of pulmonary pressure. This elevated pressure can affect the pulmonary circulation, an increase of the LAP (left atrial pressure) is often associated to 'alveolar-capillary stress failure'. It is the result of a barotrauma altering the endothelial permeability of the pulmonary capillary bed, this produce the leakage of fluid leading to pulmonary congestion and alveolar oedema[54]. LV dysfunction, mainly through PH, can result in right ventricular (RV) dysfunction and failure. Indeed, the elevation of pulmonary pressure and pulmonary vascular resistance (PWR) produces an increase of RV afterload leading to the dilatation and the shape change of right heart chambers and tricuspid regurgitation. In turn, this results in elevated RAP and ultimately in RV failure[54].

Relation between the left-side filling pressure and the right-side filling pressure

The estimation of left ventricular filling pressure (LVFP) is one of the most important measure in order to asses HF and to evaluate the evolution of the disease. Following the international guidelines, it can be measured non-invasively using a validated algorithm based on several echographic parameters. It classifies the LVFP in two classes: normal pressure (NP) and high pressure (HP), the latter is associated to worse outcome.

In a significant proportion of patients (up to 23 %) this evaluation can't be done due to impossibility of correctly assessing the necessary parameters [40]. Several studies have shown a good correlation between right atrial pressure and LVFP or PCWP in both patient with HF with reduced ejection fraction (HFrEF) and in those with HF with preserved ejection fraction(HFpEF) [18] [17][46]. Using this relation it would be possible to determine the LVFP class also for patient with unavailable echographic parameters.

Congestion assessment in HF

Congestion is one of the most frequent cause of hospitalization for patient with HF and available data have shown that patients with persistent congestion at the discharge have poor outcome and a twofold increase in 180-day mortality. For this reasons, the diagnosis of congestion and its treatment through an appropriate fluid therapy is fundamental in patient with HF. It is possible to define two kind of congestion: the first one is called clinical congestion and it is characterized by an high left ventricular diastolic pressure (LVDP) and sign and symptoms of congestion like dyspnoea, rales and oedema. The second is the haemodynamic congestion and it is associated to high LVDP with no sign and symptoms of congestion. The latter can be the prelude of clinical congestion, in fact it precedes clinical congestion by days or weeks. It may also contribute to the worsening of chronic heart failure[8]. Thus, the early detection of high filling pressure and the assessment of congestion could be very important in the prognosis of a patient with HF. The gold standard to asses congestion is the measure of RAP and PCWP.[15]

One of the most widely used classifications to assess the the hemodynamic state of a patient is the one suggested by Dr. Lynne Stevenson. It characterizes the patient on the basis of the volume status (wet or dry) and the perfusion status (warm or cold). The volume status is determined using PCWP, a patient is defined wet if PCWP is ≥ 22 mmHg otherwise the patient is considered dry. Similarly, a patient is said to be cold if the cardiac index (CI) is $\leq 2.2 \frac{l}{min \cdot m^2}$, otherwise the patient is defined warm.

Several studies have shown that the Stevenson classification can provide prognosis information, a patient that at the discharge is still classified as wet or cold is associated with an higher risk of rehospitalization or death than a patient classified

as dry and warm. This classification can also be used to establish the therapy for different kind of patient.[58]

Although, as said before, there is a strong relation between RAP and PCWP which implies that an increase of RAP reflects a rise of PCWP, there is a discordance of this two parameters in 25-30 % of patients. For this reason, recently, a new method of classification has been proposed. It suggests to evaluate the volume status of a patient on the basis of left-side filling pressure (PCWP) and right-side filling pressure (RAP). In this way it would be possible to distinguish patient with right- or left-side volume overload reflected by an high filling pressure. However, other studies are needed in order to understand if this classification can be use full to better distinguish different kind of patient of HF and to improve outcomes.

1.5 IVC Ecography

Ecography of IVC is a widespread exam in clinical practice due to its simplicity and speed of execution and the intrinsic characteristic of ecography to not expose the patient to radiations.

The most important parameter measured during IVC ecography is its diameter. Following the guidelines of the American Society of Echocardiography suggests to see the IVC in the subcostal view that allows to acquire both the longitudinal section and the transversal section of the vessel. The lateral view is an other possible approach but it is more difficult due to the the interposition of the ribs. This guidelines recommended to measure the diameter just proximal to the confluence of hepatic veins that is located approximately 0.5 to 3 cm to the right atrium [26].

1.5.1 Pulsatility Indices

As said in the previous section, the diameter of the IVC changes during the respiratory cicle, in particular, it reaches its maximum at the end of the expiration and its minimum at the end of inspiration.

The Caval Index (CI) asses the pulsatility of the IVC and it is calculated es the ratio between the differences of the maximum and mininum diameters and the the maximum diamter:

$$CI = \frac{D_{max} - D_{min}}{D_{max}} \quad (1.15)$$

Nakamura et al. shows the importance of the cardiac activity on the pulsatility of the IVC, the cardiac caval index (CCI) accounts of the IVC cardiac variation [47]. The respiratory caval index (RCI), proposed by Kircher et al., indicates the percentage of collapse of the IVC after a deep inspiration [28].

1.5.2 Use of IVC ecography in the clinical practice

The combination of IVC diameter and CI is used to determine the right atrial pressure (RAP) or the central venous pressure (CVP) that are very important parameters to assess the volume status, to evaluate the cardiac functionality and the preload.

The most accurate way to measure RAP and CVP is the catheterization, however, it is an invasive procedure that exposes the patient to several risks like infections, hemorrhage, arrhythmias, and thrombosis. Instead, IVC ultrasound represents a safe and non-invasive method to assess CVP and RAP.

Following the guidelines mentioned above, a diameter at the end of expiration > 2.1 cm and a CI $< 50\%$ are associated to high RAP, a diameter < 2.1 cm and CI $> 50\%$ are related to a normal RAP and a diameter < 2.1 cm and CI $< 50\%$ are associated to an intermediate RAP [26].

The guidelines and their updates point out that this method is less reliable for intermediate values of pressure and the necessity to combine this approach with other methods in order to correctly evaluate the right atrial pressure.

Moreover, it should be noted that this technique to assess RAP can't be used for patients being ventilated with positive pressure. However, an IVC diameter ≤ 12 mm seems to suggest a RAP < 10 mmHg in this group of patients. The IVC diameter can also be dilated in young athletes without indicating an high right atrial pressure [26].

Nowadays, the ultrasound of IVC is applied in particular in the emergency departments to evaluate the volume status. Hypovolemia is a frequent condition in critical ill patients and the responsiveness to fluid resuscitation is crucial to guide clinicians in the choice of the proper therapy. In the past, static parameters that characterize preload such as CVP and pulmonary artery occlusion pressure were used to determine fluid responsiveness, however, several studies have demonstrated that they are poor predictors of the response to a fluid challenge. Indeed, recent studies point out the reliability of the parameters extracted from IVC ultrasound as predictor of fluid responsiveness. In particular, a study of Airapetian et al. showed that a CI $> 42\%$ is a predictor of a positive response to a fluid infusion and so on an increase of cardiac output (CO) [6]. Also in the field of emergency departments, the studies of Yamaoğlu et al. and Kajimoto and al. suggest the use of IVC ecography to distinguish cardiac causes from pulmonary ones in patients that present acute dyspnea. It can be used to guide the choice of the initial therapy in combination with other exams [33] [62]. Recently, IVC ultrasound is also employed in chronic medicine, especially in the follow-up in patients undergoing hemodialysis, in order to evaluate their volume status [13].

1.5.3 Limitations of IVC ecography

Despite IVC ecography is widely employed by clinicians in different fields as said in the previous section, it still shows same limitations. In spite of the existence of international guidelines, like those of American Society of Echocardiography mentioned above, there is a lack of standardization of the exam [42].

A study of Blehar et al. shows the relative movement of IVC relative to the transducer during the respiratory cycle. In particular, the vein moves both in cranio-caudal direction and medio-lateral direction. This study stressed a mean caudal displacement of the IVC of 21.7 mm significantly higher than the lateral one which was of 3.9 mm [11]. Considering that pulsatility indices are calculated using two measure of diameter (one at the end of expiration and one at the end of inspiration) it is clear if the measure diameters correspond of different sections or there is a movement of the mid-line, the value of the index will be incorrect.

Usually, the maximum and the minimum diameters are measured using the M-mode or the B-mode, both approaches have limitations. The M-mode fail to measure the two diameter in the same section and the B-mode require that the operators to manually select the section along with calculating the diameter and, at the same time, to follow the movement of the vessel [43]. Thus, this kind of exam is highly operator-dependent.

Moreover, the diameter of IVC as well as its shape is not uniform along its course through abdomen; this is also reflected in the variability of pulsatility indices along different sections. [43] [11]

An other issue consists of the irregularity of the shape of IVC much different from a circle or an ellipsoid and the variability of the pulsatility in the different directions, especially for hypo-volemic patients. [43]

All this factors should be considered when the ecography of IVC is employed in order to obtain reliable results.

1.6 The Respiratory System

1.6.1 Anatomy of the respiratory system

The main function of the respiratory system is obviously the respiration but it is important also in regulating the acid-base balance of the blood, in protecting the organism against pathogens and in the phonation [57]. The respiration is the sum of four main process: the movement of the air inside (inspiration) and outside (expiration) of the lungs, the exchange by diffusion of oxygen and carbon dioxide between pulmonary air cavities and blood, the transport by blood of oxygen and carbon dioxide and the exchange by diffusion of this two molecules between blood and tissues.

The most important organs of the respiratory system are the lungs that are located

in the chest cavity protected by the rib cage which is constituted by 12 ribs. The chest wall is formed, other than the rib cage, by the stern, the thoracic vertebrae, the muscles, and connective tissues. The muscles responsible for the respiration are the internal and external intercostal muscles and the diaphragm which is a dome shape muscle that bounds inferiorly the chest cavity. The right lung is divided in three lobes while the left one in two. Each lung is coated by the pleural sac: the pleura is a membrane constituted by two sheet, the visceral one is attached to the lungs which is connected to the thoracic wall. The two pleural sheets are separated by a thin cavity called pleural cavity which is normally filled with 10-20 mL of plueral liquid, fundamental for the pulmonary expansion [57].

Air reaches the lungs through the upper airways and a series of conducts called respiratory tract. After entering through the oral oral nasal cavity, air passes into the pharynx and then into the larynx which is connected to the trachea. It is conduct with a diameter of about 2.5 cm and a length of 10 cm, trachea is always open thank to the presence of 15-20 C-shape incomplete cartilaginous rings conferring structural rigidity. The trachea divides into the primary bronchi, inside the lungs each of the divides into secondary bronchi, two for left lung and three for right lung. Each secondary bronchus branches into tertiary bronchi which in turn branch in smallore bronchi. As the diameter decreases, the amount of cartilage decreases. When the tubules have a diameter of less than 1 mm are called bronchioles. There about 20-23 levels of ramification that product a total of about 8 milions of tubules. The bronchioles branches into terminal bronchioles which are connected to respiratory bronchioles. They conduct air into alveolar ducts terminating in the alveoli where the gas exchange take place. Gas exchange is facilitated by the alveoli's thin wall and their large number. There are about 300 milions of alveoli which form a total surface of about 100 m^2 [57].

1.6.2 Respiratory mechanics

The flow of air inside and outside the lungs is guided by the pressure gradient between the alveoli and the external environment. Inspiration occurs when the pressure of alveoli is lower than atmospheric pressure conversely expiration takes place when the pressure of alveoli is higher than that of the external environment. There are four pressure that are crucial to describe the respiratory mechanics:

- Atmospheric pressure (P_{atm}): pressure of the external environment, it can be considered constant and equal to 760 mmHg.
- Intra-alveolar pressure (P_{ip}): pressure inside the alveoli, at rest is equal to P_{atm} but it varies during the respiratory cycle determining the pressure gradient responsible of the air flow.
- Intrapleural pressure (P_{ip}): pressure inside the pleural sac. At rest is equal to

756 mmHg, it is always lower than P_{alv} . It's always negative during normal respiration because opposite forces tend to divide the parietal pleura from the thoracic wall. Indeed, the thoracic wall is compressed trying to expand itself like a spring, on the other hand the lungs are full of air and expanded so their fibers tend to contract them.

- Transpulmonary pressure ($P_{alv} - P_{ip}$): It is a measure of the distension force of the lungs, an increase of this pressure produce an expansion of the alveoli.

The airflow is described with the following equation [57]:

$$F = \frac{P_{atm} - P_{alv}}{R} \quad (1.16)$$

The pressure gradient at numerator is created by muscles that modify the volume of the chest cavity and in turn the pressure. Indeed, the Boyle Law states that the pressure is inversely proportional to the volume: as the volume increases the pressure decreases.

The intra-alveolar pressure is determined by two factors: the volume of the alveoli and the amount of air stored inside them (measured in moles).

Inspiration

During inspiration diaphragm contract by flattening and lowering, the combined action of the internal intercostal muscles which expand the rib cage produces an increase of the volume of the chest cavity. It is reflected on the decrease of the intrapleural pressure, due to the higher strain on the parietal pleura, and in turn it produces an increase of the transpulmonary pressure. The distension of the lungs occurs and the volume of alveoli rises with a consequent decrease of the intra-alveolar pressure. The air enter the lungs until P_{ip} returns equal P_{atm} .

Exhalation

Exhalation is a passive process that don't require the contraction of any muscles during quiet breathing. Indeed, the chest wall and the lungs are elastic structure thus at the end of inspiration they tend to contract. This is reflected on a decrease of the volume and in turn on rise of the intra-alveolar pressure. Like during inspiration, the air comes out of the lungs until P_{ip} returns equal P_{atm} .

Pulmonary compliance and airways resistance

The pulmonary compliance is the change of lungs volume produced by a certain change of the transmural pressure [57].

$$C = \frac{\Delta V}{\Delta(P_{alv} - P_{ip})} \quad (1.17)$$

An higher pulmonary compliance is reflected in a minor pressure gradient required to move a certain volume of air and so on a smaller contraction of inspiration muscles.

The total resistance of airways is influenced by the value of single resistance which depends on the their radius: as the radius increases resistance decreases. A small resistance implies that the difference between P_{atm} and P_{alv} does not have to be high to produce the air flow.

1.7 Pulmonary diseases

Pulmonary diseases compromise the physiologic lungs function with an impairment of the gas exchange and an alteration of the respiratory mechanics. They are the third cause of death in the world after cardiac diseases and cancer. [20] Moreover, pulmonary disease have a strongly negative impact on the lifestyle and life expectancy. [55]

They are divided into two categories: obstructive pulmonary diseases and restrictive pulmonary diseases.

1.7.1 Obstructive pulmonary diseases

There are two main kind of chronic obstructive pulmonary disease (COPD): chronic bronchitis and emphysema. They are called "obstructive" because they are characterized by an augmented obstruction to air flow [25] that can be asses using several clinical exams that will be described in the following sections.

Smoking is considered the most important risk factor followed by exposure to pollutants and the presence of bronchial hyperactivity. The most common symptoms of COPD are dyspnea, cough and expectorion that is more frequent and abundant in patient with chronic bronchitis. In the advanced states of the pathology, barrel chest, lip and nail cyanosis may occur. [25]

Emphysema is characterized by a significant rise of the lungs volume caused by an increase of aleveoli dimensions. It ends up with the rupture of the alveoli wall reducing the available surface for the gas exchange which will be result impaired.[1] The course of the disease change a lot among different patients and it leads to the decline of the respiratory functionality.

1.7.2 Restrictive pulmonary diseases

Restrictive pulmonary diseases are a large group of diseases marked by inflammation and successive fibrosis of the pulmonary interstitial [2]. This process often interests also alveoli, terminal bronchioles and the vascular and lymphatic endothelium. It result in a decreased pulmonary compliance, a stiffer lung requires a bigger pressure gradient to move the same volume of air. There are many risk factors due to the variety of clinical presentations of this desease, the most important are the following [2]:

- Smoke
- Asbestosis
- Aspiration pneumonia
- Pnuemonia caused by drugs or radiations

- Rheumatoid arthritis, ankylosing spondylitis, and Sjögren's syndrome
- Exposure to environment pollutants such as silica and beryllium
- Genetic risk factors

Dyspnea that can occur also at rest conditions and non-productive cough are common symptoms of fibrosis. In the advanced phases of the disease fatigue and weight loss may arise. Often in the terminal state of the fibrosis patients show up pulmonary hypertension characterized by a mean pressure in the pulmonary artery higher than 25 mmHg [54].

1.7.3 Diagnostic Instrumentation

Spirometry

Pulmonary diseases cause a variation of the physiological lung volume or the speed at which air enters and leaves the lungs. Spirometry is an exam to measure such volume and flow rate in addition to lung capacities defined as sum of at least two pulmonary volumes. These values are used by the clinician to diagnose the presence of a pulmonary disease, moreover, they are very useful to distinguish between obstructive and restrictive pulmonary diseases.

First spirometers were built using a reversed bell filled with air that was immersed in a container filled with water. As the inspiration occurs the volume of air inside decreases and the bell plunges, conversely during exhalation the bell tends to move toward the surface. These movements are recorded on a paper thanks to a system of pulley that connects the bell to a pen.

Modern spirometers use a transducer that converts the air volume into an electric signal that is recorded by a computer. [57]

The most important pulmonary volumes and capacities which are calculated during spirometry are [57]:

- Tidal Volume (TV): volume of air that enters and leaves the lungs during a single respiration act (500 mL)
- Inspiratory reserve volume (IRV): volume of air that can be inhaled at the end of a normal inspiration (3000 mL)
- Expiratory reserve volume (ERV): volume of air that can be exhaled at the end of a normal exhalation (1000 mL)
- Residual Volume (RV): volume of air that is still in the lungs after a maximal exhalation (1200 mL)
- Inspiratory capacity (IC): maximum volume of air that can be inhaled after a normal expiration. $IC = TV + IRV$ (3500 mL)

- Vital Capacity (VC): maximum air volume that can be exhaled after a maximal inspiration. $VC=TV+IRV+ERV$ (4500 mL)
- Residual functional capacity (RFC): volume of air that is inside the lungs after a normal exhalation. $RFC=ERV+RV$ (2200 mL)
- Total lung capacity (TLC): volume of air inside the lungs at the end of a maximal exhalation. $TLC=TV+ERV+IRV+RV$
- Forced vital capacity (FVC): the patient executes a maximal inspiration and after that a maximal exhalation as quickly as possible.
- Forced expiratory volume (FEV1): maximum volume exhaled in 1 second

Tiffeneau Index (TI) is another important index that can be calculated from these volumes and capacities, it is the ratio between FEV1 and FVC and physiologically it is about 70-80 %. TI decreases in obstructive diseases [25] while it is unvaried in restrictive diseases due to the decrease of both FVC and FEV1.

Chest X-ray

It is one of the first exams conducted on a patient with a suspected pulmonary disease. It is possible to evaluate the central airways, the heart with the principal vessels and the diaphragm in the lower part. Clinicians can assess eventually alteration of the lung parenchyma with possible signs of chronic bronchitis or pulmonary fibrosis.

Chest High Resolution Computed Tomography (HRCT)

It is considered the gold standard combined with the spirometry to distinguish between obstructive and restrictive pulmonary diseases. CT makes possible a detailed study of the parenchyma allowing to evaluate the extensions of the lung tissue damage. Often the patient with restrictive diseases shows nodular opacity while a lowering and a flattening of the diaphragm are present in patients with obstructive diseases. The latter may show bubbles which are signs of emphysema.

Echography

Different kinds of echography are used to diagnose a pulmonary disease and in its follow-up.

Chest ultrasonography allows to evaluate the interface between visceral and parietal pleura which is a unique, horizontal, hyperechogenic line. In patients with a restrictive disease B lines, typical of pulmonary oedema, are present also without clinical signs of heart failure and the basal-apical gradient that characterizes oedema.

Instead, echocardiography permits to assess the cardiac structure and to do some quantitative measurements such as the ejection fraction (EF) and the pressure in the pulmonary artery (PAPs). The latter is estimated through the evaluation of the higher speed of tricuspid valve regurgitant flow.

Recently, IVC echography has been used in the clinical evaluation of patient pulmonary pathologies. IVC reflects intra-thoracic and abdominal pressure and its compliance is also related to the volume status as well as to the pressure in the right cardiac chambers.

Arterial blood gas test

It consists of an arterial blood draw which gives important information such as, oxygen partial pressure PaO_2 , carbon dioxide partial pressure $PaCO_2$ and pH. Altered values are signs of an impaired gas exchange reflected in acid base imbalances such as acidosis and alkalosis. Moreover, this test allows to understand the origin of these imbalances (metabolic, respiratory or mixed) and to distinguish between type I respiratory failure and type II respiratory failure:

- Type I: $PaO_2 < 55$ mmHg which implies an inadequate oxygen supply
- Type II: $PaO_2 < 55$ mmHg and $PaCO_2 > 45$ mmHg which means an inadequate oxygen supply and a difficulty to correctly remove CO_2

6 Minutes Walking Test (6MWT)

The patient has been asked to walk for 6 minutes, the level of blood oxygen saturation (SpO_2) is monitored using a saturimeter.

At the end of the time, the distance walked and the nadir of SpO_2 are measured. This test gives important information about the ability to perform daily activity.

1.7.4 Restrictive pulmonary diseases vs Obstructive pulmonary diseases

Respiratory mechanics is altered in both diseases but in different ways: the increased resistance to airflow typical of obstructive diseases causes a decrease of FEV1 and an accumulation of air known as "air-trapping".

The typical lungs of a patient with an obstructive disease are stiffer than normal ones with a reduced compliance. Thus, they can't expand enough and all volumes and capacities measured with spirometry are reduced. For these reasons, the Tiffenau Index is reduced in obstructive diseases and normal or increased in restrictive ones. Patients with both diseases, especially fibrosis, tend to develop pulmonary hypertension which is reflected on altered pressure in right heart chambers.

Indeed, the low level of oxygen in blood stream causes vasoconstriction that, in

turn, determines an elevated pressure in right ventricle and right atrium. As time goes by, it leads to cardiac hypertrophy and, ultimately, heart failure.

1.8 VIPER Software

The aim of the software developed by VIPER srl is the tracking of IVC edges both on longitudinal view and transverse view on ultrasounds videos in order to obtain more reliable estimations of caval indices and IVC diameters. It was used in several studies in which its efficiency and reliability was proven.

Its working principles are described in the following section by distinguish between longitudinal and transverse view.

1.8.1 Longitudinal view

At the start frame the user is asked to give some information and settings [42] [44]:

- The user must select two reference points which are assumed to be the anchoring sites of the vein. The left point, usually, is located near the confluence of the hepatic vein into IVC. The right one, is closer to the lower hepatic region or near the confluence between IVC and portal vein.
- The users have to define the leftmost diameter by selecting two points on the upper and lower border of the vessel.
- The users have to select the rightmost diameter drawing a line

The software starts the processing drawing 30 lines transversal to the vein and uniformly spaced between the two selected diameters. The image is pre-processed in order to enhance the contrast using different techniques suitable for the different situations that may occur. A median filter can be applied, it consists in a sliding window across the image in which value of the central pixel is replaced with the median of the other pixel values that are contained in the windows. In this way, it is possible to reduce the image noise. The vein borders are estimated on each of this 30 lines by detecting abrupt change in pixel intensity. It is possible that more than one points show a sharp change in intensity, the point closest to the one selected in the previous line is chosen. In order to smooth the edges, for each line the border position is recalculated as the mean between the original value and the linear interpolation of its two closest neighbours. The estimation of the displacement of the two reference point from one frame to the next is obtained by the comparison of the image portion with size 128x128 pixel centered on the position of reference point in the first frame of the pair. The two image portions are aligned in the 2-D Fourier domain to improve resolution [44]. From the third frame on, three frames were considered: the current one and the two previous ones. The

movements between the first and the third frame was computed as the sum of the displacement between the first and second frame and the displacement between the second and the third frame. Using the new positions of the reference points a new reference segment is drawn. The 30 lines transversal to IVC section are recalculated keeping constant the angle between each one and the reference segment and the ratio between the intersection point and the the length of the reference segment. Using this method, it is possible to follow movements and deformation of the vessel and to intersect the IVC in the same cross sections[42].

The midline of the IVC is computed by averaging the positions of the upper and lower edge for each line, then they are interpolated with a parabolic function. After that, 21 point are uniformly distributed along the midline excluding the 5% at the start and at the end in order to avoid possible edge effects. Thus, 21 diameters perpendicular to the midline were drawn in these positions[42]. They are then used in order to calculate caval indices as will be explained later.

1.8.2 Transverse view

At the first frame for the transverse view the user is asked to to select only a point that represents the center of the vein. The pre-processing of the image is the same used in the longitudinal view. The default settings of the software provides the application of a median filter with a 5x5 pixel window.

Then, 30 equidistant rays are drawn from the center of IVC. Considering that the inside portion of the vein is black and the border is considerably clearer, the border of IVC is estimated searching a point with an abrupt change in pixel intensity for each ray.

After that, the calculated point are evaluated in order to remove possible outliers using a distance criterion. The points that passes the test are polar interpolated obtaining the final estimation of the edge in the transverse section. If the number of of points rejected is higher than 15, the border of the current frame is considered equal to the one of the previous frame. This method provide a more stable estimation of the edge.

For each frame the area bounded by the estimated border is computed from which the equivalent diameter is calculated doing the root square of the area.

1.8.3 Estimation of CI,CCI and RCI

As said in the previous sections, in addition to the caval index (CI) recent studies have point out the usefulness of the respiratory caval index (RCI) which accounts of the diameter variation due to a sniff and the cardiac caval index (CCI) which evaluates the diameter variation related to cardiac activity.

Each of the them is calculated as ratio between the difference between the maximum and the minimum diameter and the the maximum diameter. First of all, it is

thus necessary to separate the cardiac component and the respiratory one from the original diameter signal. The starting point, both for longitudinal and transverse view, is the original diameter signal: in order to reduce noise, it is filtered using a Chebyshev type I low-pass filter with a cut-off frequency of 5 Hz (stopping band starting at 6 Hz, minimum attenuation of 30 dB, pass band from 0 to 5 Hz with ripple of 0.5 Hz) . Using the filtered signal, the maximum and the minimum are extracted ensuring that the distance between two subsequent maxima or minima was almost the half of the sample rate. This peaks are then interpolated to obtain the respiratory component of the diameter.

The cardiac component is computed subtracting the respiratory component from the mean diameter. Then, a component which accounts for the slow sub-respiratory fluctuations is added to the signal. It is extracted applying a low-pass filter with a cut-off frequency of 0.05 Hz (Chebyshev type I, stop band starting at 0.5 Hz, minimum attenuation of 30 dB, pass band from 0 to 0.05 Hz with ripple of 0.5 dB) to the cardiac component [19]. If the original diameter signal does not contain too much noise it is possible to use the such signal instead of the filtered one for the calculation of the cardiac component. Maxima and minima are searched on the three components and then their value and position are interpolated in order to obtain three signal of maxima and minima with the same sample rate of the original diameter signal.

CI,CCI and RCI are calculate applying the formula $\frac{D_{max}-D_{min}}{D_{max}}$ for each frame respectively to original, cardiac and respiratory signals. Finally, the mean value of each index is computed averaging the signal between the positions of the first and the last maximum or minimum, in order to avoid possible edge effects.

Chapter 2

Statistical Analysis of caval indices in pneumological patients

2.1 Statistical Sample

A total of 10 patients were involved in this study from different structures: University of Turin Directed Complex Facility of Pneumology (directed by Prof. C. Albera), its ambulatory structures (Prof. P. Solidoro) and Azienda Ospedaliera Univaersitaria (A.O.U.), Città della Scienza e della Salute of Turin, in the period between November 2021 and April 2023.

All patients were over the age of 18 years old, the mean age expressed as mean \pm was 62.1 ± 10 years. Each patient had been diagnosed with obstructive or restrictive pulmonary disease following interanational guidelines. In particular, 5 of them were obstructive and 5 restrictive. A control group of 19 patients from the department of internal medicine 1U (directed by Prof. M. Porta) without pulmonary diseases was used.

2.2 IVC ultrasounds

All Us scans were done using MyLab Eight system (Esaote, Genova, Italy, frame rate 30 Hz, 256 gray levels) with a convex probe 2-5 MHz.

Subcostal approaches was the most used, as suggested by international guidelines, because it allows to to see the IVC region between the confluence of hepatic veins and the right atrium, both in longitudinal and transversal view. The intercostal approach was used only on two patients, it is more difficult to perform due to the presence of the ribs. Clips were recorded in B-mode for a period of time of about 15-20 s in order to include more respiratory cycles.

US scans were processed using the software developed by VIPER srl whose function principle was illustrated in previous sections, after the three caval indeces and three

diameter components (total, cardiac and respiratory) were calculated using the algorithm described above.

2.3 Methods used for the statistical analysis

First of all, as said in the dedicated section, the mean value of the time series of CCI,RCI and CI was calculated excluding the first and the final part the signal in order to obtain a more stable estimation avoiding possible edge effects. Instead, the mean value of the three components of the diameter were obtained by averaging the all signal.

Thus, for each patients were computed both in longitudinal and transversal view the following parameters as mean values:

- CCI
- RCI
- CI
- Total diameter
- Respiratory diameter
- Cardiac diameter

Moreover, standard deviation, kurtosis and skewness were calculated for each diameter component of each patients both in longitudinal and transversal view, reported in table 2.1 and 2.2.

2.3.1 Boxplot

Boxplot of the distributions of caval indices and diameters were realized for the three classes: obstructive (O), restrictive (R) and the control group (C).

This graph report the 25 and 75 percentile, the median and the eventual outliers and it allows to see possible difference between the distribution of a determined parameter of different classes [3].

2.3.2 Wilcoxon Tests and Bland-Altman Plot

Wilcoxon rank sum test is a non parametric test for two populations independent populations. It test the null hypothesis that medians of the two population are the same against the alternative hypothesis that they are different.[23] [29] It was used to find any statistically significant differences between the different parameters of the different classes both in longitudinal and transverse view.

ID	Cardiac component				Respiratory component				Mean diameter			
	Std	Kur	Skw	Med	Std	Kur	Skw	Med	Std	Kur	Skw	Med
1	0.50	3.66	0.32	11.05	0.49	2.66	-0.79	11.22	0.65	3.05	-0.39	11.16
11	0.94	2.46	-0.49	12.07	1.11	1.78	0.08	11.63	1.79	2.15	-0.43	11.91
18	1.64	4.47	-0.31	13.63	3.19	2.04	-0.33	14.03	3.55	3.52	-0.76	14.22
3	0.91	4.63	1.23	14.04	0.48	22.12	2.76	14.02	0.69	5.66	0.25	14.10
4	0.41	3.47	0.34	13.93	0.63	1.98	-0.12	13.96	0.77	2.46	-0.17	13.91
5	0.94	3.81	-0.31	16.04	1.34	1.90	-0.31	16.10	1.81	2.48	-0.83	16.68
6	0.49	3.21	0.83	8.95	0.66	2.41	-0.61	9.34	0.74	2.49	-0.41	9.23
7	1.00	1.92	0.08	12.16	0.69	4.18	-0.90	12.23	1.36	2.24	-0.19	12.31
8	0.83	2.73	-0.20	6.68	0.90	2.77	0.15	6.67	1.34	2.52	0.01	6.82
9	0.74	2.40	-0.07	14.18	0.69	2.14	-0.22	14.25	0.90	2.47	-0.21	14.12
10s	0.77	3.11	-0.23	13.06	2.92	1.63	-0.44	13.79	3.12	2.08	-0.61	13.89
11s	0.46	2.67	-0.27	13.25	0.74	2.30	-0.33	13.23	0.85	3.19	-0.51	13.29
12s	1.94	2.09	0.35	14.13	1.37	2.55	0.07	14.10	1.63	2.36	-0.02	13.85
13s	1.45	2.78	0.00	10.19	1.58	2.12	-0.47	10.65	2.32	1.66	-0.21	10.95
14s	0.54	2.92	-0.08	7.21	0.68	3.02	-0.77	7.33	0.88	3.05	-0.75	7.44
15s	0.38	6.39	-1.40	9.39	1.14	1.81	-0.47	9.72	1.30	2.05	-0.58	9.76
16s	0.46	3.02	0.15	18.79	0.95	2.53	-0.77	18.97	1.03	2.43	-0.64	18.98
17s	0.65	3.05	0.35	11.28	0.25	7.71	0.81	11.21	0.61	2.83	0.02	11.28
18s	1.72	2.49	0.35	14.52	2.98	2.03	-0.55	15.26	3.32	1.86	-0.32	14.59
19s	0.88	2.75	-0.01	12.75	1.05	2.15	-0.69	13.14	1.37	3.35	-0.95	13.15
1s	0.78	2.55	0.48	14.76	0.62	2.25	-0.32	15.09	1.02	2.83	-0.24	14.90
2s	0.64	3.45	-0.51	12.34	0.76	1.54	-0.33	12.49	1.02	3.43	-0.91	12.48
3s	0.72	2.31	-0.04	15.50	1.24	2.12	0.14	15.72	1.59	1.98	-0.30	15.93
4s	0.45	2.47	-0.05	12.31	0.59	2.82	-0.69	12.48	0.80	2.46	-0.43	12.48
5s	0.46	2.78	0.16	8.64	0.52	2.30	-0.17	8.65	0.72	3.17	0.44	8.57
6s	0.59	2.27	0.00	13.93	0.37	4.04	-0.82	14.01	0.69	3.57	-0.26	13.90
7s	0.85	4.13	0.39	13.02	1.02	1.77	-0.13	13.34	1.36	2.94	-0.49	13.34
8s	0.68	2.50	-0.06	20.17	0.89	4.09	-0.82	20.02	0.98	5.10	-1.11	20.15
9s	0.86	3.16	0.69	7.10	1.30	1.56	-0.07	7.29	1.58	2.29	0.35	7.19

Table 2.1. Standard deviation (Std), kurtosis (Kur), skewness (Skw) and median (Med) for the three diameter components in longitudinal view

On the other hand, Wilcoxon signed rank test was used to find statistically significant different between the value of the same caval index on longitudinal view and on transversal view. Indeed, it is a non parametric test for two populations when observation are paired. It tests the null hypothesis that difference of the medians of the two distributions is null against the alternative hypothesis that it is not. [23]

ID	Cardiac component				Respiratory component				Mean diameter			
	Std	Kur	Skw	Med	Std	Kur	Skw	Med	Std	Kur	Skw	Med
1	0.48	3.31	-0.38	13.92	0.51	3.00	-0.92	14.04	0.70	3.08	-0.71	14.01
11	1.71	3.06	-0.53	13.77	2.27	3.74	0.92	12.78	2.93	3.37	0.41	12.97
18	1.25	3.00	0.50	12.93	2.99	1.88	-0.37	13.86	3.36	1.88	-0.52	14.46
3	1.50	3.23	0.17	10.88	2.40	2.12	0.10	10.60	3.02	1.79	0.15	10.45
4	0.55	5.46	-0.39	18.46	0.81	2.70	-0.33	18.48	1.01	3.52	-0.47	18.55
5	3.35	4.97	-1.65	19.20	5.03	9.95	-2.85	19.22	4.87	11.40	-3.02	19.36
6	0.86	3.30	0.84	10.13	1.96	1.77	-0.47	10.69	2.16	1.98	-0.59	10.98
7	1.02	2.28	-0.03	14.83	1.37	2.57	-0.51	15.02	1.66	2.64	-0.51	14.90
8	1.22	2.45	0.12	13.65	1.03	2.30	0.11	13.57	1.83	2.12	-0.14	13.86
9	1.15	2.82	-0.29	15.84	0.98	2.28	-0.36	15.74	1.67	2.59	-0.66	16.10
10s	0.41	6.15	-0.97	13.93	0.96	1.55	-0.16	14.00	1.11	2.26	-0.39	14.12
11s	0.66	3.13	-0.02	11.85	0.94	2.29	0.56	11.67	1.19	2.51	0.46	11.68
12s	0.94	2.72	-0.29	19.51	1.14	1.73	0.12	19.28	1.62	2.00	-0.05	19.64
13s	1.51	3.32	-0.73	13.06	1.89	3.15	-0.78	13.22	2.78	2.24	-0.75	14.09
14s	1.81	2.67	-0.59	13.04	1.83	2.19	-0.33	12.71	2.42	2.44	-0.57	13.23
15s	0.58	3.01	-0.36	10.80	1.49	5.43	-1.74	11.30	1.60	5.33	-1.74	11.23
16s	0.43	3.41	-0.64	20.30	0.54	2.15	-0.54	20.32	0.68	3.16	-0.73	20.39
17s	1.31	2.52	-0.17	17.31	1.06	2.23	0.34	17.04	1.77	2.36	-0.32	17.19
18s	2.69	2.69	0.36	18.36	3.40	2.10	-0.53	19.63	4.22	2.13	-0.44	19.73
19s	0.76	2.89	-0.35	13.35	0.89	1.71	0.06	13.28	1.27	2.16	-0.28	13.36
1s	0.94	2.37	-0.04	16.91	1.05	2.32	-0.19	17.19	1.43	2.77	-0.17	17.08
2s	1.40	3.68	0.74	18.58	1.32	8.28	1.54	18.56	1.48	6.19	0.47	18.76
3s	0.96	4.15	-1.18	16.71	1.32	2.37	-0.71	16.74	1.79	4.05	-1.35	17.03
4s	0.78	3.12	-0.31	13.59	0.73	1.74	0.14	13.53	1.05	2.79	0.39	13.51
5s	0.95	3.21	0.04	9.16	1.03	2.12	-0.61	9.20	1.34	2.55	-0.68	9.44
6s	0.75	4.17	-0.28	16.27	0.48	2.75	0.73	16.11	0.85	3.85	-0.50	16.30
7s	0.76	3.28	-0.42	13.58	0.68	3.50	-0.51	13.61	1.03	3.41	-0.41	13.71
8s	0.75	3.00	0.26	18.75	1.87	2.48	-0.03	18.45	1.94	2.62	0.18	18.36
9s	0.68	2.83	0.38	7.91	0.63	3.58	-0.45	8.23	0.89	3.03	0.34	7.90

Table 2.2. Standard deviation (Std), kurtosis (Kur), skewness (Skw) and median (Med) for the three diameter components in transversal view

Moreover, Bland-Altman plots were realized to better investigate the difference between the values of the caval indices in longitudinal and transversal view.

On this graph, the means of the paired measures are reported on x-axis while the difference between the two measures are shown on the y-axis. Four horizontal lines are drawn on the graph: the black solid lines corresponds on the null difference and on the mean differences. The two green dashed lines delimit the confidence interval

and they are calculated as: mean difference \pm 1.96 times the differences standard deviation.

The points that are inside the the confidence interval indicates two measures that does not show significant difference among them. The more points are distributed close to the line of the null mean, the more similar the two measures are to each other [4].

2.4 Results

Boxplot

Boxplot of the distribution of CCI, RCI and CI both for longitudinal and transversal view are shown below as well as those of mean diameter:

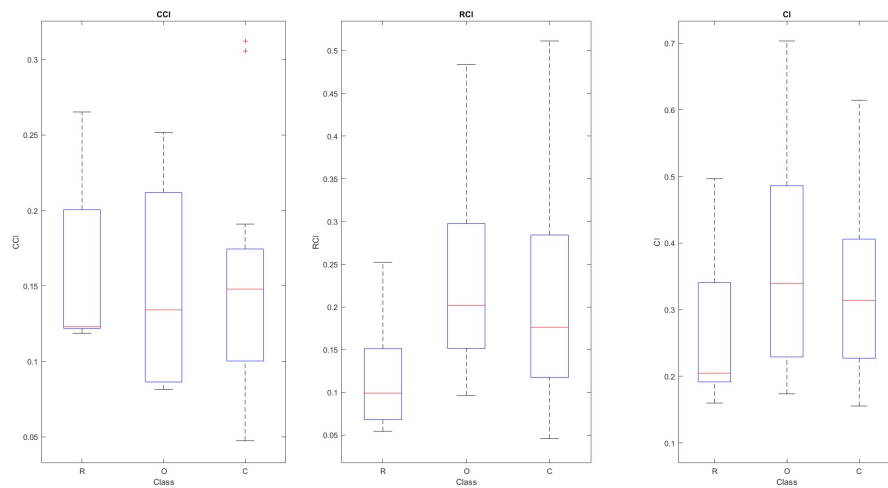


Figure 2.1. Distribution of caval indices in longitudinal view.

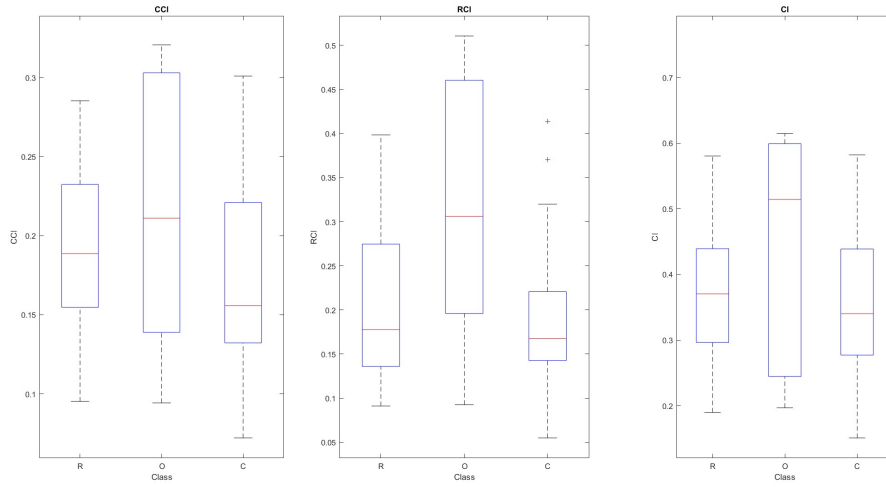


Figure 2.2. Distribution of caval indices in transversal view.

	Longitudinal			Transversal		
	R	O	C	R	O	C
CCI	0.12	0.13	0.15	0.19	0.21	0.16
RCI	0.10	0.20	0.18	0.18	0.31	0.17
CI	0.2	0.34	0.31	0.37	0.51	0.34

Table 2.3. Median value of caval indices

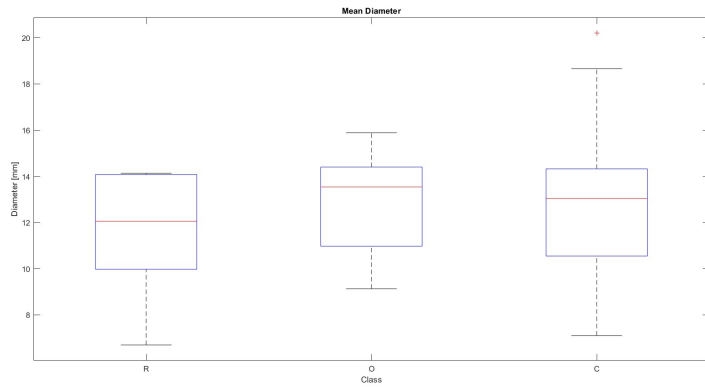


Figure 2.3. Distribution of the mean diameter in longitudinal view.

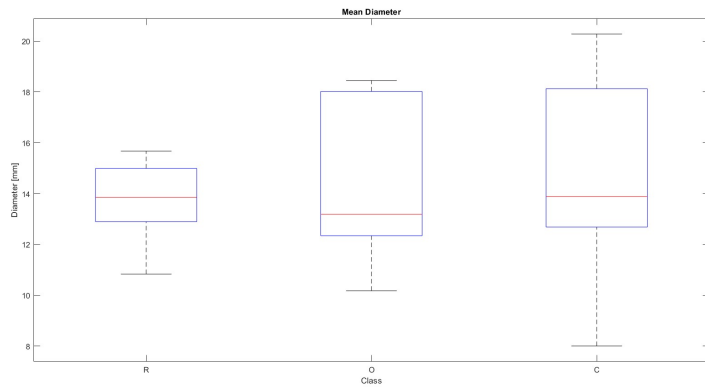


Figure 2.4. Distribution of the mean diameter in transversal view.

	Longitudinal			Transversal		
Median	R	O	C	R	O	C
Mean Diameter [mm]	12.1	13.5	13.0	13.9	13.2	13.9

Table 2.4. Median value of mean diameter

Wilcoxon rank sum Test

Wilcoxon rank sum test was computed for all indices among the different class evaluating all possible combinations. Moreover, pathological subjects were compared to control group.

The following table show the p-value of the comparisons for the different caval indices:

	Longitudinal	Transversal
p-value comparison O-R		
CCI	0.8413	0.8413
CI	0.4206	0.5476
RCI	0.2222	0.3095
p-value comparison R-C		
CCI	0.8311	0.5223
CI	0.3197	0.7223
RCI	0.1179	0.7762
p-value comparison O-C		
CCI	1	0.3555
CI	0.7223	0.4772
RCI	0.6697	0.1021
p-value comparison PAT-C		
CCI	0.9698	0.5205
CI	0.6232	0.6776
RCI	0.2730	0.4274

Table 2.5. p-value of Wilcoxon rank sum test

Wilcoxon signed rank Test

The Wilcoxon signed rank test was conducted for each caval indices to evaluate statistically significant differences between the longitudinal and the transversal view. The table below show the p-value obtained:

p-value Longitudinal-Transversal comparison	
CCI	0.0267
CI	0.0856
RCI	0.3581

Bland-Altman Plot

As said before, Bland-Altman Plot of the three caval indices were realized in order to better understand the differences between the longitudinal and transversal view. Here, they are shown:

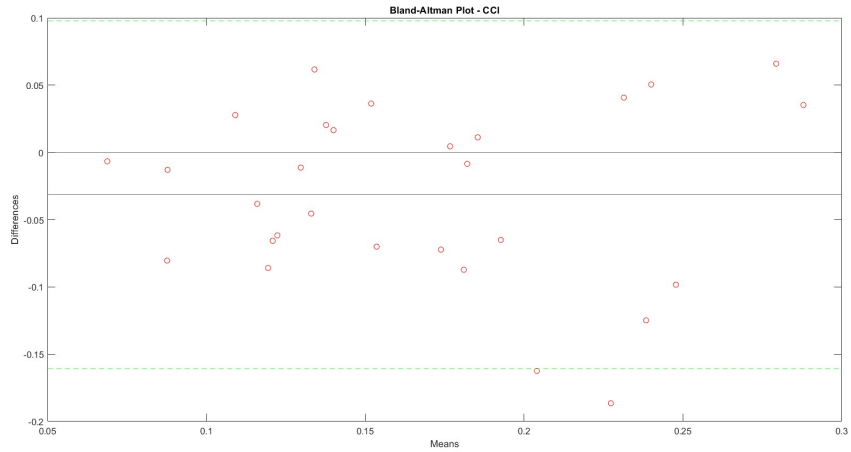


Figure 2.5. Bland-Altman Plot for the comparison between the longitudinal and the transversal view for CCI.

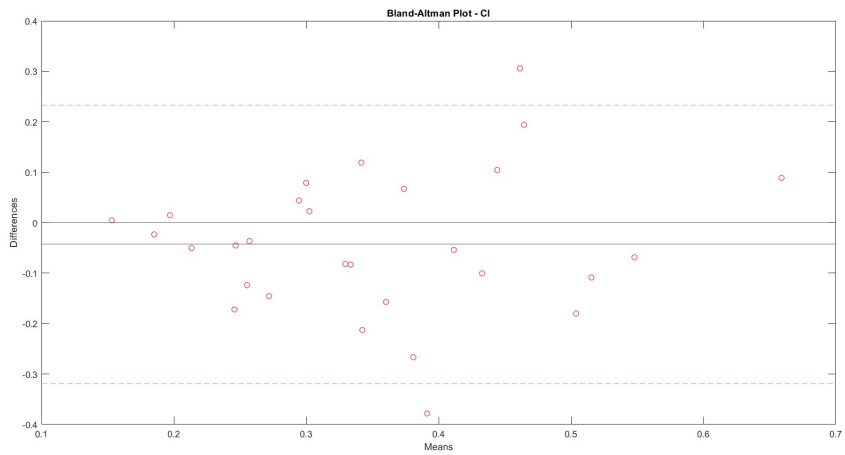


Figure 2.6. Bland-Altman Plot for the comparison between the longitudinal and the transversal view for CI.

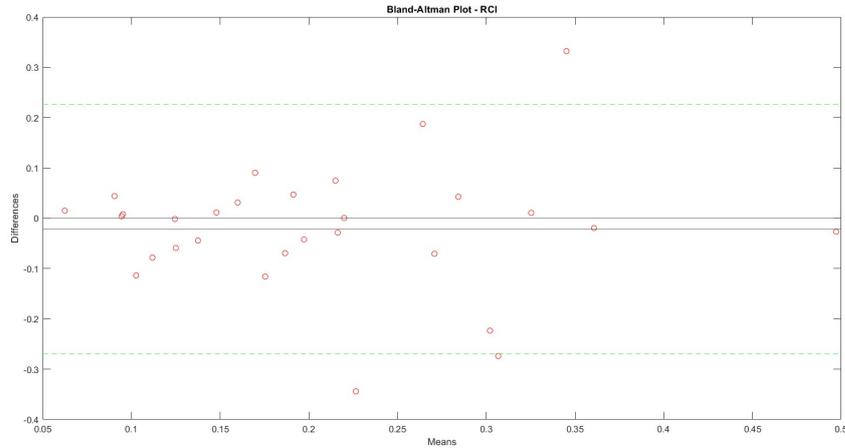


Figure 2.7. Bland-Altman Plot for the comparison between the longitudinal and the transversal view for RCI.

2.5 Discussion

The boxplot in figure 2.1 and 2.2 and the value of median reported in table 2.3 shows that there are not significant differences in the distributions of caval indices among the three classes. This observation is confirmed by the p-value of the Wilcoxon rank sum test: they are all greater than 0.05 thus, it is possible to assert that there are not statistically significant differences. The same consideration can be done about diameters that almost don't show variations between the three classes.

Although, some other observation can be done about the different distribution of the caval indices between obstructive and restrictive disease. It can be seen that all the three indices are greater in obstructive patients.

As suggested by clinicians who are studying the same problem on these subjects, this difference can be explained by the different way on which the two disease affect the pressures of the thoracic and abdominal cavity.

Patients with BPCO trap a great amount of air in the lungs and lower significantly the diaphragm, on the other hand, restrictive patients have lungs that are not able to expand enough with reduced lungs volume and capacity.

In general, in patients with restrictive disease the endothoracic pressure is increased while the abdominal is normal, this is reflected in lower pulsatility of the IVC and thus in a reduced RCI and CI. Otherwise, in obstructive patients the endothoracic pressure is normal while the abdominal one is increased this determines a greater drain of the IVC with a consequent higher pulsatility that is, in turn, reflected on greater RCI and CI.

The difference in CCI can be explained by the tendency of restrictive patients to develop pulmonary hypertension that in turns causes a rise of the right atrial

pressure. This is reflected in a lower venous return and thus in lower pulsatility of the inferior vena cava.

It should be noted that the Wilcoxon signed rank test and the Bland-Altman Plot show considering discrepancies between the longitudinal and the transversal with a statistically significant difference for the CCI (p-value < 0.05). It may be explain by the fact that in the longitudinal view a larger portion of vein in analyzed while in transversal view just one section is considered.

Chapter 3

Cardiovascular System Model

3.1 Introduction to mechanics of the cardiac cycle

The cardiac cycle is characterized by several mechanical events that determine its division different phases [35]:

- Right atrium (RA) contraction
- Left atrium (LA) contraction
- Left ventricle (LV) begins contraction
- Mitral valve closure
- Right ventricle begins contraction
- Tricuspid valve closure
- Pulmonary valve aperture
- Aortic valve aperture
- Aortic valve closure
- Pulmonary valve closure
- Tricuspid valve aperture
- Mitral valve aperture

Cardiac cycle is divided into two main phase: systole which corresponds on the ventricular contraction and diastole which is referred to ventricular filling. Systole starts with the closure of the mitral valve followed by the isovolumic phase. The ventricle begins to contract and the pressure increases but the aortic valve is still closed. It opens when the ventricular pressure exceeds the aortic one and rapid ejection occurs. As a result of ejection pressure in the ventricle decreases, when it becomes smaller than that in the aorta the aortic valve closes.

Diastole is defined as the period of time between the aortic valve closure and the mitral valve closure. The first phase of diastole is called rapid filling and in physiological conditions it accounts for the majority of ventricular filling. During this phase the atrial pressure plunges. During the slow filling the filling rate of the ventricle decrease and the atrial and the ventricular pressure are similar. Ventricular filling in this phase is strongly related to the blood returning from the lungs in the left ventricle or the the venous return in the right ventricle. Finally, atrial systole occurs, at rest in normal individual it accounts only for a minor part of blood but in diseased heart or during exercise its contribution is more important [35].

3.1.1 The Wiggers Plot

It was invented by Dr. Carl Wiggers who decided to put together atrial, ventricular and arterial pressure in order to give a clear representation of the correlation of this three important pressure during systole and diastole. Often the pressure traces are superimposed to ECG signal and ventricular volume in order to illustrate the timing and the relation of the events that significantly characterize the cardiac cycle [35].

3.1.2 Pressure-Volume Loop (PV Loop)

The pressure volume loop show graphically the relationship between pressure and volume in a determined cardiac chamber during the cardiac cycle. It was introduced for the first time in 1895 by Otto Frank and recent studies shows is usefulness to evaluate the cardiac mechanics both in research and clinical application reported in the review of Bastos and al. [31] On this graph it is possible to identify the four most important phases of the cardiac cycle: isovolumetric contraction, ejection, isovolumetric relaxation and passive filling. Moreover some significant values of volume and pressure are easily detectable such as:

- Systolic Pressure
- Diastolic Pressure
- End-systolic pressure
- End-diastolic volume (EDV)
- End-systolic volume (ESV)
- Stroke volume (SV) = EDV-ESV

As showed in figure 3.1, P-V loops can provide other important information about cardiac mechanics and efficiency beyond those mentioned before such as: the end-diastolic pressure volume relationship, the end-systolic pressure volume relationship, contractility and stiffness of the cardiac chambers and arterial elastance.

Moreover, the total mechanical energy is equal to the P-V area and it the sum of the stroke work which is the work implied for ventricle contraction in a single beat (red area, inside the P-V loop) and the residual potential energy of the myocardium cells at the end of the systole (blue area, on the left of P-V loop)[31].

3.2 Lumped parameters models

The term "lumped parameters" refers to the properties of the system to be divided in discrete elements or components in which them properties are concentrated and

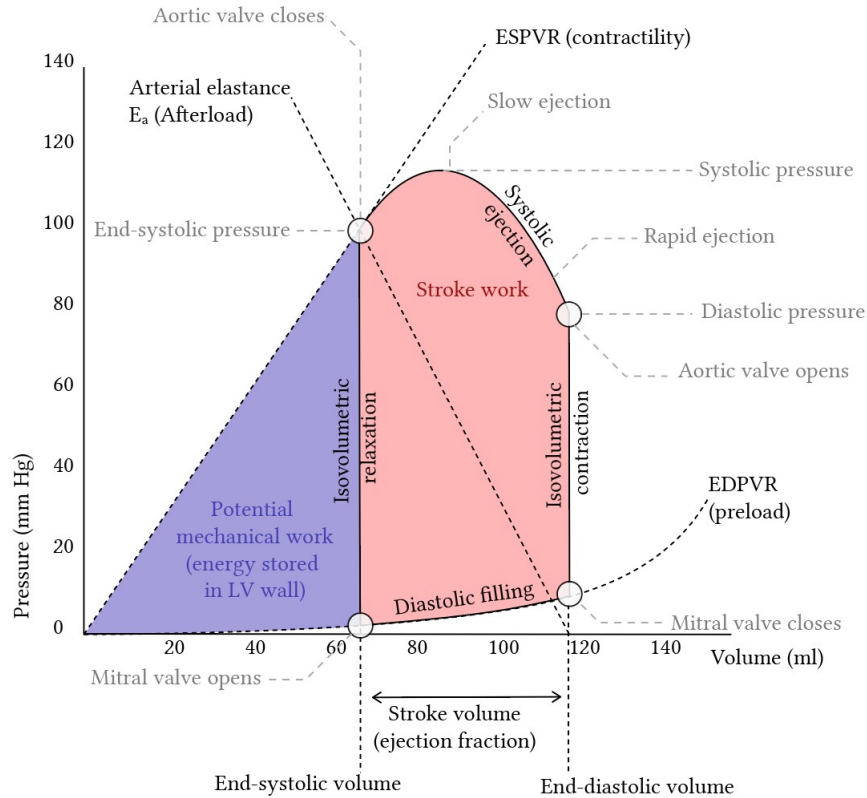


Figure 3.1. Stylized version of a P-V Loop [5].

well defined, rather being distributed among the space. This approach allows to use simple mathematical model to describe the behaviour of the system such as ordinary differential equations (ODE). Searching the literature, it can be seen lumped parameters are widely adopted to model the cardiovascular system [10] [49] [50] [61] [27] [14] [12]. Often, it is modeled using an equivalent hydraulic circuits and the equation employed for the mathematical solutions are based on the analogy between hydraulic components and electrical ones which will be discussed in the following section.

As suggested by Barnea et Al. cardiovascular system can be modeled using lumped parameters obtaining reliable estimation of pressures and volume. Thus, it is possible to avoid to use Navier-Stokes equation and those that describe elastic wall motion that would require more complex mathematical solutions and higher computational cost. The same considerations can be done about the hearth, it can be represented using finite elements solving the equations in each elements. On the other hand, a lumped parameters model can describe the contractility activity of the heart as unique system with reasonable values of pressures and volumes [10].

3.2.1 Analogy between cardiovascular system and electrical circuits

As said before, there is a significant correspondence between the parameters and the the variable that are used to describe the cardiovascular system and those of an electrical circuit. Indeed, pressure, volume of blood and flow rate correspond respectively to potential, electric charge and current [63].

Vessel Resistance

The vessel resistance can be related to flow and pressure as the electrical resistance is related to current and potential using the Ohm's law [63]:

$$R_v = \frac{\Delta P}{F} \quad (3.1)$$

Vessel Compliance

Arteries and veins are compliant, they are able to accumulate and release blood during the different phases of the cardiac cycle thanks to the elastic wall. Such properties can be described using the current-voltage relation of a capacitor[63]:

$$F = C_v \frac{dP}{dt} \quad (3.2)$$

Blood inertia

Blood mass resists to flow due to pressure gradient in a vessel, similarly an inductor avoids instant current changes. Thus, the pressure-flow relation can be expressed as[63]:

$$P = L_v \frac{dF}{dt} \quad (3.3)$$

Heart Valve

Heart valves regulate the flow rate from a atria to ventricles and from ventricle to arteries. Their aperture and closure is regulated by pressure difference, for example if the atrial pressure exceeds the ventricular pressure, the atrio-ventricular valve is open and it opposes a small resistance to blood flow, otherwise it is closed. Heart valves can be modeled as ideal diode[63]:

$$\begin{cases} 0 & \text{if } \Delta P < 0 \\ \frac{P}{R} & \text{if } \Delta P \geq 0 \end{cases} \quad (3.4)$$

Change in volume over time

The conservation of mass under steady-state flow corresponds on Kirchhoff's voltage and current laws and it can be written a[63]:

$$\frac{dV}{dt} = F_{in} - F_{out} \quad (3.5)$$

3.3 Method

The mathematical model implemented in Matlab R2022a is based on the on the system of ordinary differential equations (ODE) developed by Ursino et al. [61] in order to solve the hydraulic circuit that represent the cardiovascular system (CVS). It is constituted by two closed loops to describe systemic and pulmonary circulations and a time-varying elastance model for the ventricles. Such model has been integrated with others in order to more realistically depict the variables and the parameters that characterize CVS.

The equation employed will be discussed in detail in the following sections.

3.3.1 Equations for the vascular compartments

Ursino et al. divided systemic circulation is divided into 5 compartments, in addition to the two more compartments were added to describe the abdominal and thoracic IVC, as it follows:

- Systemic arteries (subscript sa)
- Splanchnic peripheral (subscript sp)
- Splanchnic venous circulation (sv)
- Extrasplanchnic peripheral (subscript ep)
- Extrasplanchnic venous circulation (subscript ev)
- Abdominal inferior vena cava (subscript ivcA)
- Thoracic inferior vena cava (subscript ivcT)

The pulmonary circutation is described using 3 compartments:

- Pulmonary artery (subscript pa)
- Pulmonary venous circulation (subscript pv)
- Pulmonary peripheral (subscript pp)

Each vessel is characterized by three parameters: an hydraulic resistance (R), a compliance (C) and an unstressed volume (V_u), the volume at zero-filling pressure. Large arteries are described using also a value of inertance (L) to account the blood inertial effect.

For each vessel equations 3.2 and 3.1 are applied, moreover, equation 3.3 is used to describe large arteries, as it follows:

$$\frac{dP_{pa}}{dt} = \frac{1}{C_{pa}} \cdot (F_{o,r} - F_{pa}) \quad (3.6)$$

$$\frac{dF_{pa}}{dt} = \frac{1}{L_{pa}} \cdot (P_{pa} - P_{pp} - R_{pa} \cdot F_{pa}) \quad (3.7)$$

$$\frac{dP_{pp}}{dt} = \frac{1}{C_{pp}} \cdot (F_{pa} - \frac{P_{pp} - P_{pv}}{R_{pp}}) \quad (3.8)$$

$$\frac{dP_{pv}}{dt} = \frac{1}{C_{pv}} \cdot (\frac{P_{pp} - P_{pv}}{R_{pp}} - \frac{P_{pv} - P_{la}}{R_{pv}}) \quad (3.9)$$

$$\frac{dP_{ev}}{dt} = \frac{1}{C_{ev}} \cdot (\frac{P_{sp} - P_{ev}}{R_{ep}} - \frac{P_{ev} - P_{ivcA}}{R_{ev}}) \quad (3.10)$$

$$\begin{aligned} P_{sv} = & \frac{1}{C_{sv}} \cdot [V_t - C_{sa} \cdot P_{sa} - (C_{sp} + C_{ep}) \cdot P_{sp} \\ & - C_{ev} \cdot P_{ev} - C_{ivc} \cdot P_{ivcA} - C_{ivc} \cdot P_{ivcT} - V_{ra} - V_{rv} + \\ & - C_{pa} \cdot P_{pa} - C_{pp} \cdot P_{pp} - C_{pv} \cdot P_{pv} - V_{la} - V_{lv} - V_u] \end{aligned} \quad (3.11)$$

V_t is the volume of blood while V_u is the total unstressed volume:

$$V_u = V_{u,sa} + V_{u,sp} + V_{u,ep} + V_{u,sv} + V_{u,ev} + V_{u,ivc} + V_{u,ra} + V_{u,pa} + V_{u,pp} + V_{u,pv} + V_{u,la} \quad (3.12)$$

$$\frac{dP_{ivcA}}{dt} = \frac{1}{C_{ivc}} \cdot (\frac{P_{sv} - P_{ivcA}}{R_{sv}} + \frac{P_{ev} - P_{ivcA}}{R_{ev}} - \frac{P_{ivcA} - P_{ivcT}}{R_{ivc}}) \quad (3.13)$$

$$\frac{dP_{ivcT}}{dt} = \frac{1}{C_{ivc}} \cdot (\frac{P_{ivcA} - P_{ivcT}}{R_{ivc}} - \frac{P_{ivcT} - P_{ra}}{R_{ivc}}) \quad (3.14)$$

IVC Respirophasic variations

One of the most innovative part of this cardiovascular system model is the description of the respirophasic variation of the IVC diameter. During the inspiration the transmural pressure drops determining a rise of the venous return and a flow from the abdominal portion of the IVC to the thoracic one and in turn in the right atrium. In contrast, during exhalation the a blood drainage from the lower limbs take place in abdominal IVC. The influence of thoracic and abdominal pressure on IVC diameter variation is strongly related to the kind of the respiratory effort.

In order to take into account of this effect two terms were added to equations 3.13 and 3.14:

$$\frac{dP_{ivcA}}{dt} = \frac{1}{C_{ivc}} \cdot \left(\frac{P_{sv} - P_{ivcA}}{R_{sv}} + \frac{P_{ev} - P_{ivcA}}{R_{ev}} - \frac{P_{ivcA} - P_{ivcT}}{R_{ivc}} + \frac{dP_{ext,A}}{dt} \right) \quad (3.15)$$

$$\frac{dP_{ivcT}}{dt} = \frac{1}{C_{ivc}} \cdot \left(\frac{P_{ivcA} - P_{ivcT}}{R_{ivc}} - \frac{P_{ivcT} - P_{ra}}{R_{ivc}} + \frac{dP_{ext,T}}{dt} \right) \quad (3.16)$$

where $P_{ext,A}(t)$ and $P_{ext,T}(t)$ are two functions that model the action of the thoracic and abdominal pressure on the IVC.

3.3.2 Equations for the hearth

The contractility activity of ventricles and atria is described using a time-varying elastance model. Elastance is the ratio between pressure volume and it varies during the cardiac cycle, its behaviour is depicted by two relations: the end-systolic pressure/volume relationship (ESPVR) and the end-diastolic pressure/volume relationship (EDPVR).

Sagawa et Al. [32] [38], showed that at the end of the systole pressure varies linearly with volume, the slope of the line is called End-systolic elastance (E_{max}) and it is often used as indices of contractility, as the slope increases the contractility increases. [31]

Instead, during the diastole the pressure/volume relationship is exponential and it reflect the relaxation of the cardiac muscle fibers and their interaction with the surrounding tissue [61].

The four valves are modeled as ideal diode.

Left Ventricle

The change in volume of the left ventricle (subscript lv) is equal to the difference between the flow from the atrium and the the cardiac output:

$$\frac{dV_{lv}}{dt} = F_{i,lv} - F_{o,lv} \quad (3.17)$$

The term $F_{i,lv}$ is regulated by the aperture and closure of the mitral valve:

$$\left\{ \begin{array}{ll} 0 & \text{if } P_{la} \leq P_{lv} \\ \frac{P_{la} - P_{lv}}{R_{la}} & \text{if } P_{la} > P_{lv} \end{array} \right. \quad (3.18)$$

Instead, $F_{o,lv}$ depends on the movements of the aortic valve:

$$\begin{cases} 0 & \text{if } P_{max,lv} \leq P_{sa} \\ \frac{P_{max,lv} - P_{sa}}{R_{lv}} & \text{if } P_{max,lv} > P_{sa} \end{cases} \quad (3.19)$$

$P_{max,lv}$ is the isometric left ventricle pressure which accounts of the contraction or relaxation of the ventricle:

$$P_{max,lv} = \phi(t) \cdot E_{max,lv} \cdot (V_{lv} - V_{u,lv}) + [1 - \phi(t)] \cdot P_{0,lv} \cdot (e^{k_{E,lv} \cdot V_{lv}} - 1) \quad (3.20)$$

where $E_{max,lv}$ is the end-systolic elastance, $V_{u,lv}$ is the unstressed volume for the left ventricles that corresponds on the x-axis intercept of end-systolic pressure/volume relationship. $P_{0,lv}$ and $k_{E,lv}$ are two parameters that characterize the exponential pressure/volume function of the diastole.

$\phi(t)$ is a function used to switch from the systolic to the diastolic pressure/volume relationship, it varies from 0 to 1 and it is equal to 1 at maximum contraction and to 0 at the complete relaxation. Its analytical expression is the one suggested by Zhang which it is said to fit physiological data better than the one proposed by Piene et al. used by Ursino et al.:

$$\phi(t_n) = 1.553174 \cdot \left[\frac{(\frac{t_n}{0.7})^{1.9}}{1 + (\frac{t_n}{0.7})^{1.9}} \right] \cdot \left[\frac{1}{1 + (\frac{t_n}{1.173474})^{21.9}} \right] \quad (3.21)$$

$$t_n = \frac{t}{0.2 + 0.1555 \cdot T_{cycle}} \quad (3.22)$$

where t_n is the normalized time and T_{cycle} is the duration of a cardiac cycle. R_{lv} is the viscous resistance of the left ventricle and it varies proportionally to the isometric pressure ($P_{max,lv}$):

$$R_{lv} = k_{R,lv} \cdot P_{max,lv} \quad (3.23)$$

where $k_{R,lv}$ is a constant parameter.

Thus, the ventricle pressure is calculated as the difference between the isometric pressure and the viscous losses:

$$P_{lv} = P_{max,lv} - R_{lv} \cdot F_{o,l} \quad (3.24)$$

Right ventricle

The equation for the right ventricle (subscript rv) are the same of the those use used for the left ventricle but with different parameters and pressure involved. They are reported below:

$$\frac{dV_{rv}}{dt} = F_{i,rv} - F_{o,rv} \quad (3.25)$$

$F_{i,rv}$ is the inflow of the right ventricle and it depends on the aperture ore closure of the tricuspid valve:

$$\begin{cases} 0 & \text{if } P_{ra} \leq P_{rv} \\ \frac{P_{ra}-P_{rv}}{R_{ra}} & \text{if } P_{ra} > P_{rv} \end{cases} \quad (3.26)$$

$F_{0,rv}$ is the outflow of the right ventricle and it is regulated by the pulmonary valve:

$$\begin{cases} 0 & \text{if } P_{max,rv} \leq P_{pa} \\ \frac{P_{max,rv}-P_{pa}}{R_{rv}} & \text{if } P_{max,rv} > P_{pa} \end{cases} \quad (3.27)$$

$$P_{max,rv} = \phi(t) \cdot E_{max,rv} \cdot (V_{rv} - V_{u,rv}) + [1 - \phi(t)] \cdot P_{0,rv} \cdot (e^{k_{E,rv} \cdot V_{rv}} - 1) \quad (3.28)$$

$$\phi(t_n) = 1.553174 \cdot \left[\frac{\left(\frac{t_n}{0.7}\right)^{1.9}}{1 + \left(\frac{t_n}{0.7}\right)^{1.9}} \right] \cdot \left[\frac{1}{1 + \left(\frac{t_n}{1.173474}\right)^{21.9}} \right] \quad (3.29)$$

$$t_n = \frac{t}{0.2 + 0.1555 \cdot T_{cycle}} \quad (3.30)$$

$$R_{rv} = k_{R,rv} \cdot P_{max,rv} \quad (3.31)$$

$$P_{rv} = P_{max,rv} - R_{rv} \cdot F_{o,r} \quad (3.32)$$

Left atrium

Ursino et al. does not provide a description of contractility activity of atria, in order to more realistically characterize the pumping function of the whole heart, the atria description was taken from the model proposed by Bozkurt et al. [12] with some modifications to merge the two systems of equations.

Indeed, Bozkurt et al. used a time-varyng elastance model also for the atria but their mathematical model studied the realltion between pressure and radius of the cardiac chambers and not the more traditional one between pressure and volume like Ursino et al. Thus, the function proposed was modified in order to use a pressure/volume relation, as it follows:

$$P_{la}(t) = E_{la}(t) \cdot (V_{la}(t) - V_{0,la}) \quad (3.33)$$

where P_{la} is the pressure of the left atrium (subscript la), E_{la} is the left atrial elastance function, $(V_{la}(t))$ is the volume of the left atrium and $V_{0,la}$ is the unstressed-volume.

$$E_{la}(t) = E_{min,la} + 0.5 \cdot (E_{max,la} - E_{min,la}) \cdot \phi_{la}(t - D) \quad (3.34)$$

where $E_{min,la}, E_{max,la}$ and D are constant parameters while $\phi_{la}(t)$ is the atrial activation function:

$$\begin{cases} 0 & 0 \leq t < T_a \\ 1 - \cos\left(2\pi \frac{t-T_a}{T_{cycle}-T_a}\right) & T_a \leq t < T_{cycle} \end{cases} \quad (3.35)$$

Change in volume of the left atrium can be expressed as the difference between the the inflow and the outflow:

$$\frac{dV_{ra}}{dt} = \frac{P_{ivcT} - P_{ra}}{R_{ivc}} - F_{i,lv} \quad (3.36)$$

where $F_{i,lv}$ is the flow entering the left ventricle.

Right Atrium

As for the ventricles, also equations that describe atrial activity are very similar in the left and right side of the heart. Equations used to model right atrial (subscript ra) contractility are showed below:

$$P_{ra}(t) = E_{ra}(t) \cdot (V_{ra}(t) - V_{0,ra}) \quad (3.37)$$

$$E_{ra}(t) = E_{min,ra} + 0.5 \cdot (E_{max,ra} - E_{min,ra}) \cdot \phi_{ra}(t - D) \quad (3.38)$$

$$\begin{cases} 0 & 0 \leq t < T_a \\ 1 - \cos\left(2\pi \frac{t-T_a}{T_{cycle}-T_a}\right) & T_a \leq t < T_{cycle} \end{cases} \quad (3.39)$$

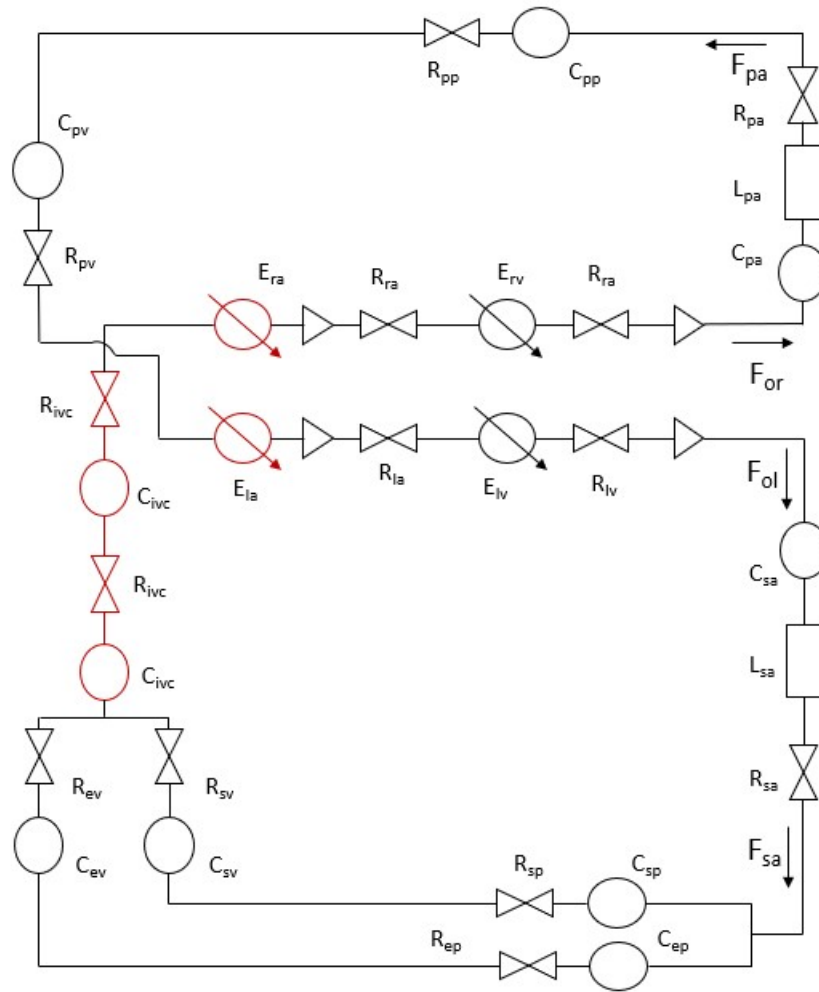


Figure 3.2. Hydraulic circuit diagram; the red parts are those modified or added respect to Ursino model.

3.3.3 Implementation of Ursino Model

Initially, Ursino model [61] was implemented on MatLab R2022a and it was tested using the parameters proposed by the author reported in tables 3.1, 3.2 and 3.3

Vascular compartments: Resistances, compliances and inertances	
Parameters	Ursino et Al. Model
R_{sa}	$0.06 \text{ mmHg} \cdot \text{s} \cdot \text{mL}^{-1}$
R_{sp}	$3.307 \text{ mmHg} \cdot \text{s} \cdot \text{mL}^{-1}$
R_{ep}	$1.407 \text{ mmHg} \cdot \text{s} \cdot \text{mL}^{-1}$
R_{sv}	$0.038 \text{ mmHg} \cdot \text{s} \cdot \text{mL}^{-1}$
R_{ev}	$0.016 \text{ mmHg} \cdot \text{s} \cdot \text{mL}^{-1}$
R_{pa}	$0.023 \text{ mmHg} \cdot \text{s} \cdot \text{mL}^{-1}$
R_{pp}	$0.0894 \text{ mmHg} \cdot \text{s} \cdot \text{mL}^{-1}$
R_{pv}	$0.0056 \text{ mmHg} \cdot \text{s} \cdot \text{mL}^{-1}$
C_{sa}	$0.28 \text{ mL} \cdot \text{mmHg}^{-1}$
C_{sp}	$2.05 \text{ mL} \cdot \text{mmHg}^{-1}$
C_{ep}	$1.67 \text{ mL} \cdot \text{mmHg}^{-1}$
C_{sv}	$61.11 \text{ mL} \cdot \text{mmHg}^{-1}$
C_{ev}	$50 \text{ mL} \cdot \text{mmHg}^{-1}$
C_{pa}	$0.76 \text{ mL} \cdot \text{mmHg}^{-1}$
C_{pp}	$5.8 \text{ mL} \cdot \text{mmHg}^{-1}$
C_{pv}	$25.37 \text{ mL} \cdot \text{mmHg}^{-1}$
C_{la}	$19.23 \text{ mL} \cdot \text{mmHg}^{-1}$
C_{ra}	$31.25 \text{ mL} \cdot \text{mmHg}^{-1}$
L_{sa}	$0.22 \cdot 10^{-3} \text{ mmHg} \cdot \text{mL} \cdot \text{s}^{-2}$
L_{pa}	$0.18 \cdot 10^{-3} \text{ mmHg} \cdot \text{mL} \cdot \text{s}^{-2}$

Table 3.1. Resistances, compliances and inertances of vascular compartments

Vascular compartments: unstressed volumes	
Parameters	Ursino et Al. Model
$V_{u,sa}$	0 mL
$V_{u,sp}$	274.4 mL
$V_{u,ep}$	336.6 mL
$V_{u,sv}$	1121 mL
$V_{u,ev}$	1375 mL
$V_{u,pa}$	0 mL
$V_{u,pp}$	123 mL
$V_{u,pv}$	120 mL

Table 3.2. Unstressed volumes of vascular compartments

Heart parameters	
Parameters	Ursino et Al. Model
$V_{u,lv}$	16.77 mL
R_{la}	$2.5 \cdot 10^{-3} \text{ mmHg} \cdot \text{s} \cdot \text{mL}^{-1}$
$k_{E,lv}$	0.014 mL^{-1}
$E_{max,lv}$	$2.95 \text{ mmHg} \cdot \text{mL}^{-1}$
$k_{R,lv}$	$3.75 \cdot 10^{-4} \text{ s} \cdot \text{mL}^{-1}$
$P_{0,lv}$	1.5 mmHg
$V_{u,rv}$	40.8 mL
R_{ra}	$2.5 \cdot 10^{-3} \text{ mmHg} \cdot \text{s} \cdot \text{mL}^{-1}$
$k_{E,rv}$	0.011 mL^{-1}
$E_{max,rv}$	$1.75 \text{ mmHg} \cdot \text{mL}^{-1}$
$k_{R,rv}$	$1.4 \cdot 10^{-3} \text{ s} \cdot \text{mL}^{-1}$
$P_{0,rv}$	1.5 mmHg

Table 3.3. Heart parameters

3.3.4 Implementation of atrial time-varying elastance and IVC description

As said in previous sections, Ursino model describe atria using only a resistance and a compliance such as vessel, in this way atrial contractility is neglected. In order to consider it the atrial time-varying elastance model proposed by Bozkurt et al. was adopted. [12]

Moreover, two vessel compartments were added to better describe IVC, dividing it in the abdominal and thoracic portions. Such as other vascular district, they were modeled using three parameters:

- R_{ivc} : the same value of resistance was adopted for both IVC portion and its

value was calculated using Poiseuille Law considering a diameter equal to 21 mm, a length of 22 cm a blood viscosity equal to 4 times water viscosity.

- C_{ivc} : its value was set considering that of right atria, decreasing it in order to consider the presence of surrounding tissue and diaphragm. Also the compliance was equal in the two IVC sections.
- $V_{u,ivc}$: the value proposed by Heldt et Al. [27] in their simulator was adopted.

The value of resistances and compliances of the the vessel compartments proposed by Ursino were modified in order to better integrate the parts of the model, as reported in table 3.6. Parameters of heart equations were the same of Ursino with the addition of those of the new equations for the description of atria (table 3.5) as well as unstressed volumes.

Vascular compartments: Resistances (R) [$\frac{mmHg \cdot s}{mL}$], compliances (C) [$\frac{mL}{mmHg}$]		
Parameters	Ursino et Al. Model	Atrial contractility and IVC model
R_{sa}	0.06	0.051
R_{sp}	3.307	2.646
R_{ep}	1.407	1.126
R_{sv}	0.038	0.030
R_{ev}	0.016	0.013
R_{pa}	0.023	0.016
R_{pp}	0.0894	0.063
R_{pv}	0.0056	0.004
R_{ivc}	/	0.0012
C_{sa}	0.28	0.308
C_{sp}	2.05	2.255
C_{ep}	1.67	1.837
C_{sv}	61.11	67.22
C_{ev}	50	55
C_{pa}	0.76	0.874
C_{pp}	5.8	6.670
C_{pv}	25.37	29.18
C_{ivc}	/	20

Table 3.4. Resistances, compliances and inertances of vascular compartments before and after the tuning of parameters

Heart parameters	
Parameters	Atrial contractility and IVC Model
$V_{u,lv}$	16.77 mL
R_{la}	$2.5 \cdot 10^{-3} \text{ mmHg} \cdot \text{s} \cdot \text{mL}^{-1}$
$k_{E,lv}$	0.014 mL^{-1}
$E_{max,lv}$	$2.95 \text{ mmHg} \cdot \text{mL}^{-1}$
$k_{R,lv}$	$3.75 \cdot 10^{-4} \text{ s} \cdot \text{mL}^{-1}$
$P_{0,lv}$	1.5 mmHg
$V_{u,rv}$	40.8 mL
R_{ra}	$2.5 \cdot 10^{-3} \text{ mmHg} \cdot \text{s} \cdot \text{mL}^{-1}$
$k_{E,rv}$	0.011 mL^{-1}
$E_{max,rv}$	$1.75 \text{ mmHg} \cdot \text{mL}^{-1}$
$k_{R,rv}$	$1.4 \cdot 10^{-3} \text{ s} \cdot \text{mL}^{-1}$
$P_{0,rv}$	1.5 mmHg
$E_{max,la}$	$0.3 \text{ mmHg} \cdot \text{mL}^{-1}$
$E_{min,la}$	$0.2 \text{ mmHg} \cdot \text{mL}^{-1}$
$v_{u,la}$	5 mL
$E_{max,ra}$	$0.3 \text{ mmHg} \cdot \text{mL}^{-1}$
$E_{min,ra}$	$0.2 \text{ mmHg} \cdot \text{mL}^{-1}$
$V_{u,ra}$	5 mL

Table 3.5. Heart parameters for the atrial contractility and IVC model

3.3.5 Modelling of the IVC respirophasic variations

As said before, IVC diameter changes in function of the transmural pressure; the influence of the thoracic and the abdominal pressure changes according to the type of breathing: thoracic or diaphragmatic.

In order to simulate a thoracic breathing the previous model was employed substituting equations 3.13 and 3.14 with equations 3.15 and 3.16. A sine wave with frequency (f_r) and amplitude equal respectively to 0.3 Hz and 2.5 mmHg was chosen. The abdominal pressure was hypothesized constant and equal to 1 mmHg.

$$P_{ext,A} = 1 \quad (3.40)$$

$$P_{ext,T}(t) = 2.5 \cdot \sin(2\pi f_r t) \quad (3.41)$$

The terms of equation 3.42 involving P_{ivcA} and P_{ivcT} were modified in order to consider the transmural pressure instead of the internal IVC pressure:

$$\begin{aligned}
 P_{sv} = \frac{1}{C_{sv}} \cdot [V_t - C_{sa} \cdot P_{sa} - (C_{sp} + C_{ep}) \cdot P_{sp} \\
 - C_{ev} \cdot P_{ev} - C_{ivc} \cdot (P_{ivcA} - P_{ext,A}) - C_{ivc} \cdot (P_{ivcT} - P_{ext,T}) \\
 - V_{ra} - V_{rv} + -C_{pa} \cdot P_{pa} - C_{pp} \cdot P_{pp} - C_{pv} \cdot P_{pv} - V_{la} - V_{lv} - V_u]
 \end{aligned} \tag{3.42}$$

At the end of the simulation diameters and volumes of both IVC sections were calculated, as it follows:

$$V_{ivc,A} = C_{ivc} \cdot (P_{ivcA} - P_{ext,A}) \tag{3.43}$$

$$V_{ivc,T} = C_{ivc} \cdot (P_{ivcT} - P_{ext,T}) \tag{3.44}$$

$$D_{ivc,A} = \sqrt{\frac{4V_{ivc,A}}{\pi L_{ivc}}} \tag{3.45}$$

$$D_{ivc,T} = \sqrt{\frac{4V_{ivc,T}}{\pi L_{ivc}}} \tag{3.46}$$

The IVC pulsatility was evaluated by calculating the caval index; it was computed for each respiratory cycle using the formula: $\frac{D_{max} - D_{min}}{D_{max}}$, then the obtained values were averaged obtaining a mean value of CI. This procedure was done for both the sections; the global CI of the whole IVC was obtained by averaging the two values.

As with the previous implementation, resistances and compliances were modified while the heart parameters and the unstressed volumes were kept the same of the former model.

Simulation of restrictive pulmonary disease

In restrictive patients the intra-thoracic pressure is increased and it is reflected in decreased drainage from lower limbs and venous return. To mimic this phenomenon the amplitude of the external thoracic pressure has been lowered:

$$P_{ext,T}(t) = 1.5 \sin(2\pi f_r t) \tag{3.47}$$

$$P_{ext,A} = 1 \tag{3.48}$$

Simulation of restrictive pulmonary disease

Obstructive pulmonary disease is characterized by an increased abdominal pressure due to the lowering of the diaphragm and a normal intra-thoracic pressure. To simulate this, a negative sine wave with amplitude greater than 1 mmHg was adopted:

$$P_{ext,T}(t) = 2.5 \sin(2\pi f_r t) \quad (3.49)$$

$$P_{ext,A} = -1.5 \sin(2\pi f_r t) \quad (3.50)$$

Vascular compartments: Resistances (R) [$\frac{mmHg \cdot s}{mL}$], compliances (C) [$\frac{mL}{mmHg}$]			
Parameters	Ursino et Al. Model	IVC respirophasic variations model	
R_{sa}	0.06		0.057
R_{sp}	3.307		2.976
R_{ep}	1.407		1.266
R_{sv}	0.038		0.034
R_{ev}	0.016		0.014
R_{pa}	0.023		0.018
R_{pp}	0.0894		0.072
R_{pv}	0.0056		0.004
R_{ivc}	/		0.0012
C_{sa}	0.28		0.308
C_{sp}	2.05		2.255
C_{ep}	1.67		1.837
C_{sv}	61.11		67.22
C_{ev}	50		55
C_{pa}	0.76		0.874
C_{pp}	5.8		6.670
C_{pv}	25.37		29.18
C_{pv}	/		20

Table 3.6. Resistances, compliances and inertances of vascular compartments before and after the tuning of parameters

3.4 Results

The values of the most important volumes and pressures were reported on graphs to show their trend during the different cardiac cycles and their maximum and minimum values were compared to the physiological ones, as showed in tables 3.7,

3.8 and 3.9.

It can be noted that all the values of pressures and volumes are within the physiological ranges [48], except the minimum value of the pulmonary artery pressure that is slightly above (3.9 % over the maximum physiological value).

Moreover, the Wiggers Plots shows that all wave forms of cardiac chamber pressures are similar to those reported in literature [35]. In particular, as showed in figures 3.7 and 3.8, the introduction of the elastance time- varying description to model atrial contractility has changed the atrial pressure traces both on the left and right side, making them more like to the physiological wave forms which are marked by the presence of two positive and two negative deflections. [35].

Figures 3.12 and 3.14 show clearly the influence of the respiration through the intra-thoracic and abdominal pressure on IVC volume and in turn on IVC diameter both in thoracic and abdominal portions. In figure 3.14 can be noted the increase of venous return during inspiration characterized by increased volume in the thoracic sections and decreased volume in the abdominal portions. The influence of respiration can be appreciated also on right-sided cardiac chamber pressures which have a different periodicity compared to those of the model in which breathing influence on IVC was not considered. The caval index calculated for the simulated thoracic breathing was equal to 0.33 which is similar to those of the control group of the study and agreed with the reference values in the literature. Also using this latest version of the model all values of the most important volumes and pressures are within the physiological range as illustrated in table 3.9.

The variations of $P_{ext,T}$ and $P_{ext,A}$ is reflected in changes of abdominal and thoracic volumes and thus in IVC diameters. It seems to reproduce the influence of intra-thoracic and abdominal pressure on IVC that can be observed in pneumological patients, despite the value of CI is quite different from those measured by US scans. This difference may be explained by the approximations adopted and by the fact that the model parameters should be adapted for each patient.

	Physiological Range [48]		Model outputs	
	Min	Max	Min	Max
Vlv [mL]	50–100	100–160	54.2	130.8
Vrv [mL]	50–100	100–160	52.8	130.6
Pla [mmHg]	2	12	6.9	8.9
Pra [mmHg]	2	8	4.2	5.7
Plv [mmHg]	5–12	90–140	5.4	123.3
Prv [mmHg]	0–8	17–32	3.3	28.9
Psa [mmHg]	60–90	90–140	89.4	123.3
Ppa [mmHg]	4–13	17–32	13.5	28.9

Table 3.7. Values of pressures and volumes using Ursino Model.

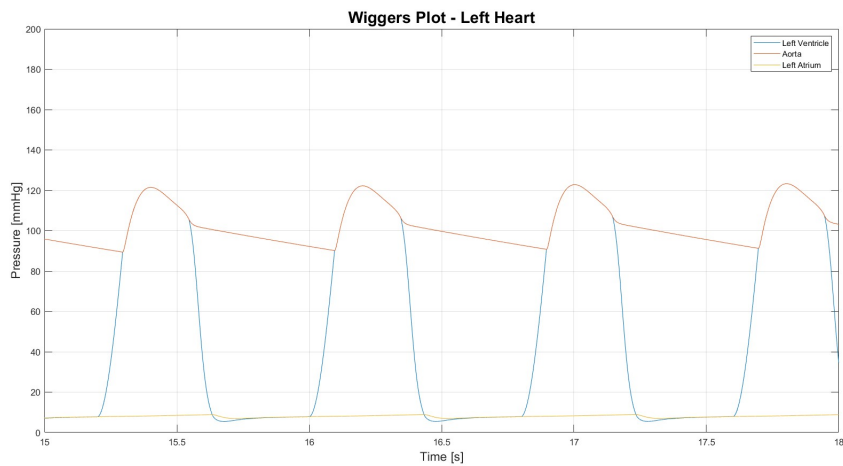


Figure 3.3. Wiggers Plot for the left heart.

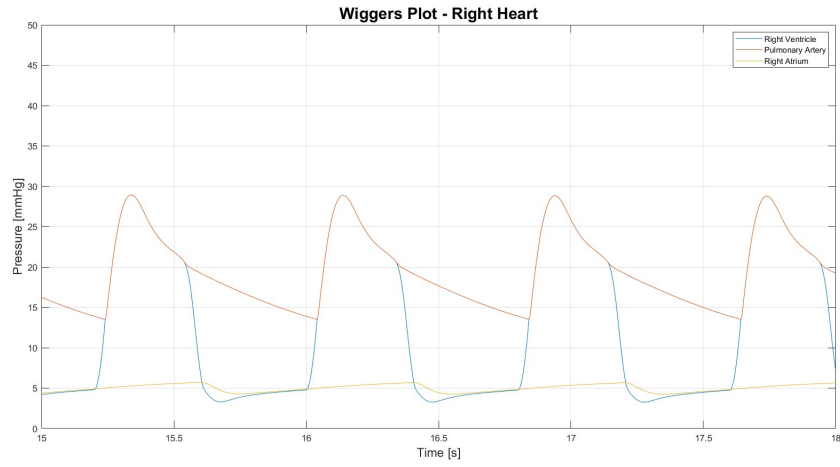


Figure 3.4. Wiggers Plot for the right heart.

	Physiological Range [48]		Model outputs	
	Min	Max	Min	Max
Vlv [mL]	50–100	100–160	50.1	133.7
Vrv [mL]	50–100	100–160	51.8	134.9
Pla [mmHg]	2	12	6.3	9.1
Pra [mmHg]	2	8	3.3	5.8
Plv [mmHg]	5–12	90–140	4.9	112.0
Prv [mmHg]	0–8	17–32	2.43	25.8
Psa [mmHg]	60–90	90–140	82.1	112.0
Ppa [mmHg]	4–13	17–32	11.5	25.8

Table 3.8. Values of pressures and volumes using atrial contractility and IVC model.

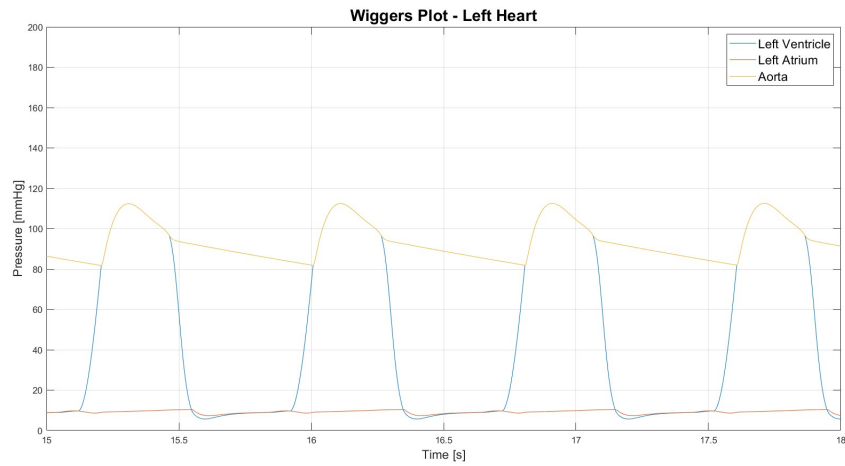


Figure 3.5. Wiggers Plot for the left heart - Atrial contractility and IVC model.

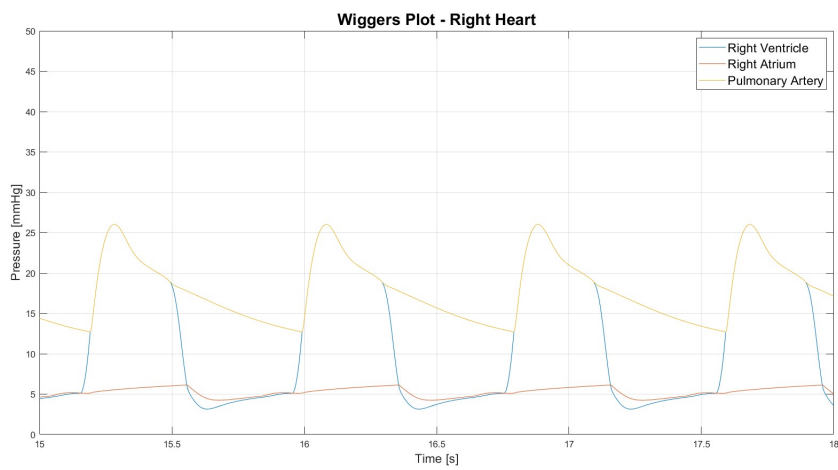


Figure 3.6. Wiggers Plot for the right heart - Atrial contractility and IVC model.

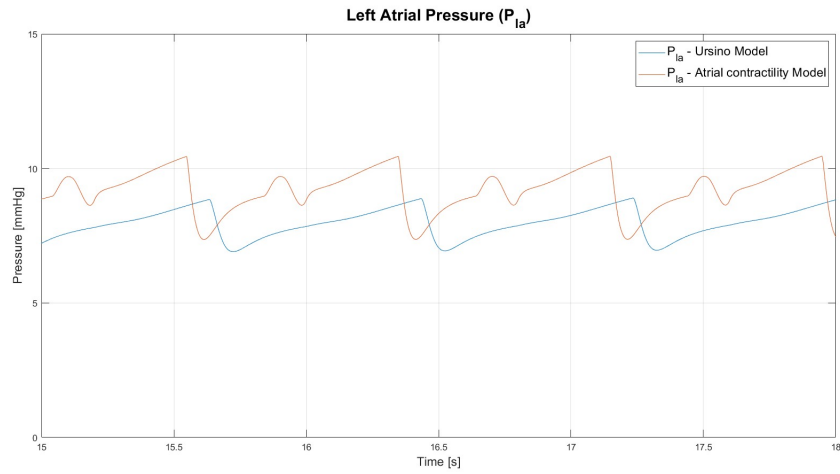


Figure 3.7. Comparison between the left atrial pressure trace obtained using Ursino model and that obtained after the implementation of the time-varying elastance model for the left atrium.

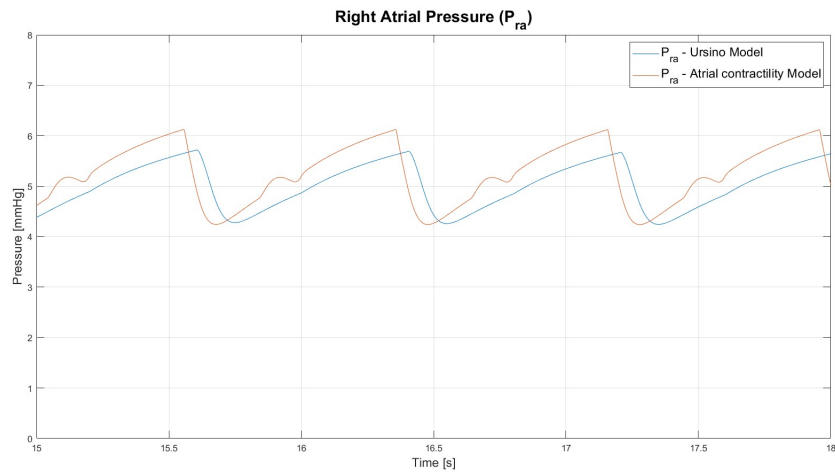


Figure 3.8. Comparison between the right atrial pressure trace obtained using Ursino model and that obtained after the implementation of the time-varying elastance model for the right atrium.

	Physiological Range [48]		Model outputs	
	Min	Max	Min	Max
Vlv [mL]	50–100	100–160	50.7	125.4
Vrv [mL]	50–100	100–160	50.5	134.1
Pla [mmHg]	2	12	6.3	10.5
Pra [mmHg]	2	8	4.2	6.1
Plv [mmHg]	5–12	90–140	5.7	112.6
Prv [mmHg]	0–8	17–32	3.1	26.0
Psa [mmHg]	60–90	90–140	81.7	112.6
Ppa [mmHg]	4–13	17–32	12.7	26.02

Table 3.9. Values of pressures and volumes using IVC respirophasic variations model.

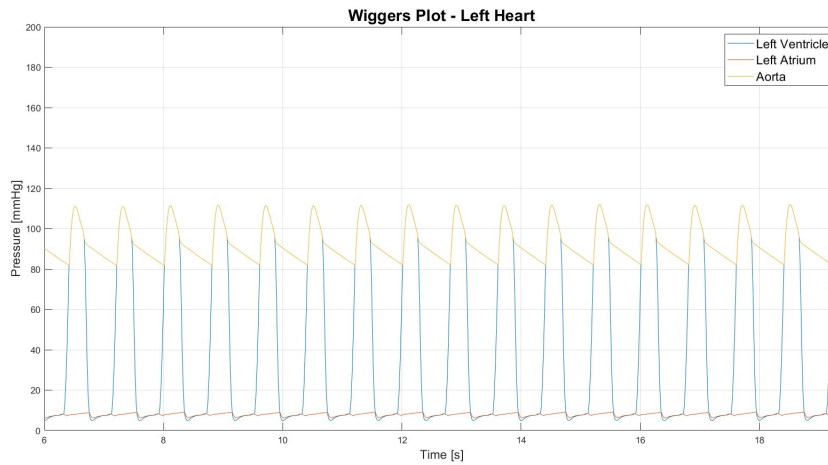


Figure 3.9. Wiggers Plot for the left heart - IVC respirophasic variations model.

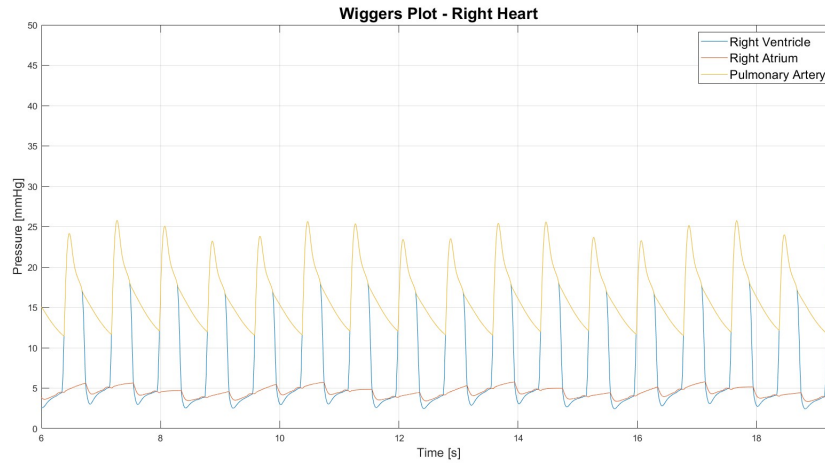


Figure 3.10. Wiggers Plot for the right heart - IVC respirophasic variations model.

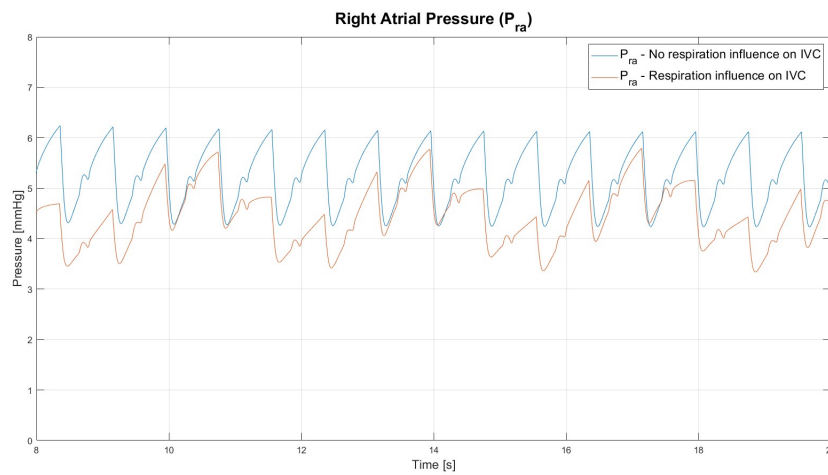


Figure 3.11. Comparison between the right atrial pressure traces with or without the influence of the respiration on IVC.

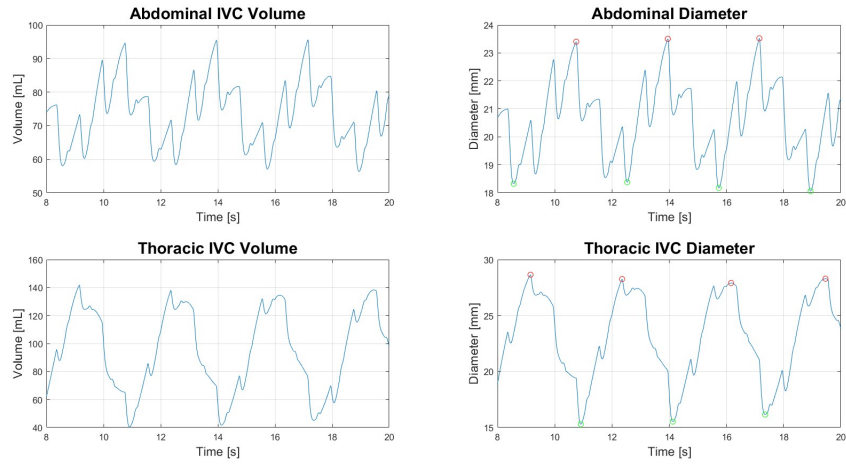


Figure 3.12. Volume and diameter of abdominal and thoracic IVC sections. Red and green dots indicate respectively maximums and minimums used for calculating CI

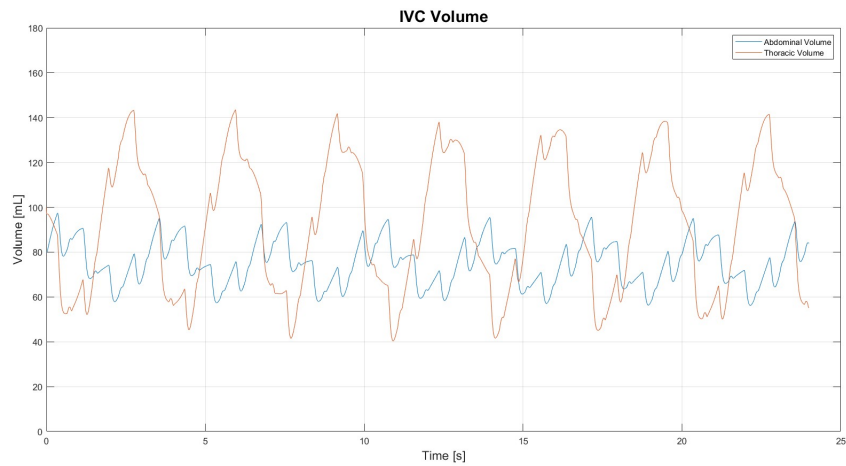


Figure 3.13. Comparison between IVC abdominal and thoracic volume.

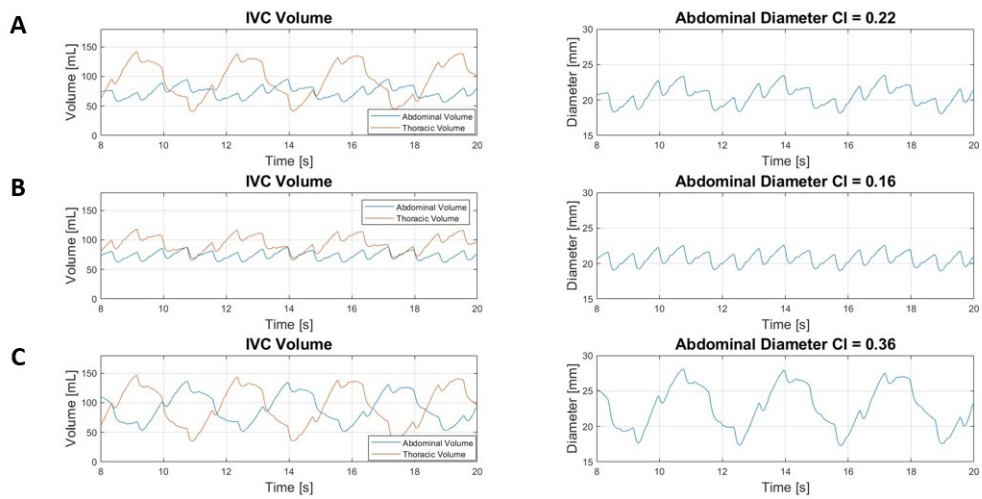


Figure 3.14. Simulations of the influence of the two types of pulmonary diseases on IVC: A) Normal (thoracic) breathing, B) Restrictive disease, C) Obstructive disease.

Chapter 4

Conclusions

Ultrasounds scan of the inferior vena cava is a powerful tool that is commonly used in different clinical area and there are several studies which are evaluating its employment in other medical fields.

On the other hand, the parameters extracted from IVC ultrasonography, such as the caval index, are not always reliable due to the inherent limitations of the examination when it is performed in the standard way. For this reasons, innovative software like that developed by VIPER srl can be very usefull to make the most of the potential of this exam.

In this work, IVC ultrasounds scans of pneumological patients were analyzed in order to investigate the possible difference in the value of the caval indices between the two class of lung diseases: obstructive and restrictive diseases. The statistical analysis showed that there are not any statistically significant difference among the two classes. The same results were obtained comparing the the distributions of the caval indices of pneumological patients with those of a control group. However, this outcome can be partly due to small size of the sample and other considerations deserve to be made. As suggested by the clinicians who are studying the same issue on this patients, the differences in the distribution of caval indices between obstructive and restrictive can be explained by the different way in which they alter the respiratory mechanics. It is reflected in changes of intra-thoracic and abdominal pressure that, in turn, influence the IVC diameter variations.

In parallel to the analysis of IVC US scans, a model of the cardiovascular system was implemented on Matlab R2022a. It was based on a model found in literature which was modified to account of atrial contraction and respirophasic variations of IVC. This model has proven to be able to reproduce the pressure and volume traces during several cardiac cycles in physiological conditions and to account of IVC diameter variations among breathing cycles. Moreover, it was used to try to reproduce the behaviour of IVC in obstructive and restrictive diseases.

In future, a more realistic versions of the functions that simulate intra-thoracic

and abdominal pressure should be adopted to model more accurately this complex phenomenon. Moreover, this model may be used to mimic other pathologies like heart failure or alteration of the volume status, such as hypohypovolemia and hypervolemia.

Bibliography

- [1] URL: <https://medlineplus.gov/emphysema.html>.
- [2] URL: <https://www.pulmonaryfibrosis.org/life-with-pf/about-pf>.
- [3] URL: <https://paolapozzolo.it/boxplot/>.
- [4] URL: <https://paolapozzolo.it/bland-altman-plot/>.
- [5] URL: <https://derangedphysiology.com/main/cicm-primary-exam/required-reading/cardiovascular-system/Chapter%2029/ventricular-pressure-volume-loops>.
- [6] Norair Airapetian et al. “Does inferior vena cava respiratory variability predict fluid responsiveness in spontaneously breathing patients?” In: *Critical Care* 19 (1 Nov. 2015). ISSN: 1466609X. DOI: [10.1186/s13054-015-1100-9](https://doi.org/10.1186/s13054-015-1100-9).
- [7] Stefano Albani et al. *Inferior Vena Cava Edge Tracking Echocardiography: A Promising Tool with Applications in Multiple Clinical Settings*. Feb. 2022. DOI: [10.3390/diagnostics12020427](https://doi.org/10.3390/diagnostics12020427).
- [8] “Assessing and grading congestion in acute heart failure: A scientific statement from the acute heart failure committee of the heart failure association of the European society of cardiology and endorsed by the European society of intensive care medicine”. In: *European Journal of Heart Failure* 12 (5 May 2010), pp. 423–433. ISSN: 13889842. DOI: [10.1093/eurjhf/hfq045](https://doi.org/10.1093/eurjhf/hfq045).
- [9] “Assessment of Phasic Changes of Vascular Size by Automated Edge Tracking-State of the Art and Clinical Perspectives”. In: 8 (Jan. 2022).
- [10] Ofer Barnea. *The Open Pacing*. 2010, pp. 55–59. URL: <http://www.eng.tau.ac.il/~barneao>.
- [11] David J Blehar et al. “Inferior vena cava displacement during respirophasic ultrasound imaging”. In: *Critical Ultrasound Journal* 4 (1 Dec. 2012). DOI: [10.1186/2036-7902-4-18](https://doi.org/10.1186/2036-7902-4-18).
- [12] Selim Bozkurt. “Mathematical modeling of cardiac function to evaluate clinical cases in adults and children”. In: *PLoS ONE* 14 (10 Oct. 2019). ISSN: 19326203. DOI: [10.1371/journal.pone.0224663](https://doi.org/10.1371/journal.pone.0224663).

- [13] J. Matthew Brennan et al. “Handcarried ultrasound measurement of the inferior vena cava for assessment of intravascular volume status in the outpatient hemodialysis clinic.” In: *Clinical journal of the American Society of Nephrology : CJASN* 1 (4 2006), pp. 749–753. ISSN: 1555905X. DOI: [10.2215/CJN.00310106](https://doi.org/10.2215/CJN.00310106).
- [14] Annual IEEE Computer Conference et al. *IEEE International Symposium on Circuits and Systems (ISCAS), 2013 19-23 May 2013, Beijing, China*. ISBN: 9781467357623.
- [15] *Congestion in heart failure: a contemporary look at physiology, diagnosis and treatment*. Oct. 2020. DOI: [10.1038/s41569-020-0379-7](https://doi.org/10.1038/s41569-020-0379-7).
- [16] Christopher Cook et al. “The annual global economic burden of heart failure”. In: *International Journal of Cardiology* 171 (3 Feb. 2014), pp. 368–376. ISSN: 01675273. DOI: [10.1016/j.ijcard.2013.12.028](https://doi.org/10.1016/j.ijcard.2013.12.028).
- [17] Mark H. Drazner et al. “Relationship of right- to left-sided ventricular filling pressures in advanced heart failure insights from the escape trial”. In: *Circulation: Heart Failure* 6 (2 Mar. 2013), pp. 264–270. ISSN: 19413289. DOI: [10.1161/CIRCHEARTFAILURE.112.000204](https://doi.org/10.1161/CIRCHEARTFAILURE.112.000204).
- [18] Mark H. Drazner et al. “The relationship of right-and left-sided filling pressures in patients with heart failure and a preserved ejection fraction”. In: *Circulation: Heart Failure* 3 (2 2010), pp. 202–206. ISSN: 19413297. DOI: [10.1161/CIRCHEARTFAILURE.109.876649](https://doi.org/10.1161/CIRCHEARTFAILURE.109.876649).
- [19] Leonardo Ermini et al. “The Cardiac Caval Index: Improving Noninvasive Assessment of Cardiac Preload”. In: *Journal of Ultrasound in Medicine* 41 (9 Sept. 2022), pp. 2247–2258. ISSN: 15509613. DOI: [10.1002/jum.15909](https://doi.org/10.1002/jum.15909).
- [20] Eurostat. *Statistiche sulle cause di morte*. URL: https://ee.europa.eu/eurostat/statistics-explained/index.php?title=Causes_of_death_statistics/it.
- [21] Paula Ferrada et al. *Qualitative Assessment of the Inferior Vena Cava: Useful Tool for the Evaluation of Fluid Status in Critically Ill Patients*.
- [22] Anna Folino et al. “Vena Cava Responsiveness to Controlled Isovolumetric Respiratory Efforts”. In: *Journal of Ultrasound in Medicine* 36 (10 Oct. 2017), pp. 2113–2123. ISSN: 15509613. DOI: [10.1002/jum.14235](https://doi.org/10.1002/jum.14235).
- [23] Chakraborti Subhabrata Gibbons Jean Dickinson. *Nonparametric Statistical Inference*. Chapman and Hall/CRC, 2010.
- [24] Guido Valli Giuseppe Coppini Stefano Diciotti. *Bioimmagini*. Patron Editore, 2012.

- [25] *Global Initiative for Chronic Obstructive Lung Disease 2023 POCKET GUIDE STRATEGIA GLOBALE PER LA DIAGNOSI, IL TRATTAMENTO E LA PREVENZIONE DELLA BPCO REVISIONE 2023*. 2022. URL: www.goldcopd.org.
- [26] *Guidelines for the Echocardiographic Assessment of the Right Heart in Adults: A Report from the American Society of Echocardiography. Endorsed by the European Association of Echocardiography, a registered branch of the European Society of Cardiology, and the Canadian Society of Echocardiography*. July 2010. DOI: [10.1016/j.echo.2010.05.010](https://doi.org/10.1016/j.echo.2010.05.010).
- [27] Thomas Heldt et al. *CVSim: An Open-Source Cardiovascular Simulator for Teaching and Research*. URL: <http://physionet.org/>.
- [28] Ronald B. Himelman et al. “Inferior vena cava plethora with blunted respiratory response: A sensitive echocardiography sign of cardiac tamponade”. In: *Journal of the American College of Cardiology* 12 (6 1988), pp. 1470–1477. ISSN: 07351097. DOI: [10.1016/S0735-1097\(88\)80011-1](https://doi.org/10.1016/S0735-1097(88)80011-1).
- [29] Chicken Eric Hollander Myles Wolfe Douglas A. *Nonparametric Statistical Inference*. John Wiley and Sons, 2014.
- [30] *Intravenous fluid therapy in the perioperative and critical care setting: Executive summary of the International Fluid Academy (IFA)*. Dec. 2020. DOI: [10.1186/s13613-020-00679-3](https://doi.org/10.1186/s13613-020-00679-3).
- [31] *Invasive left ventricle pressure-volume analysis: Overview and practical clinical implications*. Mar. 2020. DOI: [10.1093/eurheartj/ehz552](https://doi.org/10.1093/eurheartj/ehz552).
- [32] Joe Alexander Jr et al. *Instantaneous Pressure-Volume Relation of the Ejecting Canine Left Atrium*. URL: <http://ahajournals.org>.
- [33] Katsuya Kajimoto et al. “Rapid evaluation by lung-cardiac-inferior vena cava (LCI) integrated ultrasound for differentiating heart failure from pulmonary disease as the cause of acute dyspnea in the emergency setting.” In: *Cardiovascular ultrasound* 10 (1 2012). ISSN: 14767120. DOI: [10.1186/1476-7120-10-49](https://doi.org/10.1186/1476-7120-10-49).
- [34] Kambiz Kalantari et al. *Assessment of intravascular volume status and volume responsiveness in critically ill patients*. 2013. DOI: [10.1038/ki.2012.424](https://doi.org/10.1038/ki.2012.424).
- [35] Alison Keenon et al. *Cardiovascular Hemodynamics for the Clinician*. 2017.
- [36] Clinton D. Kemp and John V. Conte. *The pathophysiology of heart failure*. Sept. 2012. DOI: [10.1016/j.carpath.2011.11.007](https://doi.org/10.1016/j.carpath.2011.11.007).
- [37] Bruce J. Kimura et al. “The effect of breathing manner on inferior vena caval diameter”. In: *European Journal of Echocardiography* 12 (2 Feb. 2011), pp. 120–123. ISSN: 15252167. DOI: [10.1093/ejehocardiography/jeq157](https://doi.org/10.1093/ejehocardiography/jeq157).

- [38] W Lowell Maughan et al. *Ventricular systolic interdependence: volume elastance model in isolated canine hearts* *Ventricular systolic interdependence: volume elastance model in isolated canine hearts* Downloaded from www.physiology.org/journal 1987, pp. 1381–1390. URL: www.physiology.org/journal/ajpheart.
- [39] Theresa A. McDonagh et al. *2021 ESC Guidelines for the diagnosis and treatment of acute and chronic heart failure*. Sept. 2021. DOI: [10.1093/eurheartj/ehab368](https://doi.org/10.1093/eurheartj/ehab368).
- [40] Donato Mele et al. “Right Atrial Pressure Is Associated with Outcomes in Patients with Heart Failure and Indeterminate Left Ventricular Filling Pressure”. In: *Journal of the American Society of Echocardiography* 33 (11 Nov. 2020), pp. 1345–1356. ISSN: 10976795. DOI: [10.1016/j.echo.2020.05.027](https://doi.org/10.1016/j.echo.2020.05.027).
- [41] Luca Mesin, Stefano Albani, and Gianfranco Sinagra. “Non-invasive Estimation of Right Atrial Pressure Using Inferior Vena Cava Echography”. In: *Ultrasound in Medicine and Biology* 45 (5 May 2019), pp. 1331–1337. ISSN: 1879291X. DOI: [10.1016/j.ultrasmedbio.2018.12.013](https://doi.org/10.1016/j.ultrasmedbio.2018.12.013).
- [42] Luca Mesin, Paolo Pasquero, and Silvestro Roatta. “Tracking and Monitoring Pulsatility of a Portion of Inferior Vena Cava from Ultrasound Imaging in Long Axis”. In: *Ultrasound in Medicine and Biology* 45 (5 May 2019), pp. 1338–1343. ISSN: 1879291X. DOI: [10.1016/j.ultrasmedbio.2018.10.024](https://doi.org/10.1016/j.ultrasmedbio.2018.10.024).
- [43] Luca Mesin et al. “Automated volume status assessment using inferior vena cava pulsatility”. In: *Electronics (Switzerland)* 9 (10 Oct. 2020), pp. 1–14. ISSN: 20799292. DOI: [10.3390/electronics9101671](https://doi.org/10.3390/electronics9101671).
- [44] Luca Mesin et al. “Semi-automated tracking and continuous monitoring of inferior vena cava diameter in simulated and experimental ultrasound imaging”. In: *Ultrasound in Medicine and Biology* 41 (3 Mar. 2015), pp. 845–857. ISSN: 1879291X. DOI: [10.1016/j.ultrasmedbio.2014.09.031](https://doi.org/10.1016/j.ultrasmedbio.2014.09.031).
- [45] Alberto Oliaro Michele Loizzi. *Malattie dell'apparato respiratorio*. Edizioni Minerva Medica, 2018.
- [46] Sherif F. Nagueh et al. “Mean Right Atrial Pressure for Estimation of Left Ventricular Filling Pressure in Patients with Normal Left Ventricular Ejection Fraction: Invasive and Noninvasive Validation”. In: *Journal of the American Society of Echocardiography* 31 (7 July 2018), pp. 799–806. ISSN: 10976795. DOI: [10.1016/j.echo.2018.01.025](https://doi.org/10.1016/j.echo.2018.01.025).
- [47] Kensuke Nakamura et al. “Cardiac variation of inferior vena cava: New concept in the evaluation of intravascular blood volume”. In: *Journal of Medical Ultrasonics* 40 (3 July 2013), pp. 205–209. ISSN: 13464523. DOI: [10.1007/s10396-013-0435-6](https://doi.org/10.1007/s10396-013-0435-6).

- [48] *Normal Hemodynamic Parameters and Laboratory Values Normal Hemodynamic Parameters-Adult Normal Hemodynamic Parameters-Adult*. 2014.
- [49] Gabriela Ortiz-León, Marta Vilchez-Monge, and Juan J. Montero-Rodríguez. “Simulations of the cardiovascular system using the cardiovascular simulation toolbox”. In: vol. 36. Schloss Dagstuhl- Leibniz-Zentrum für Informatik GmbH, Dagstuhl Publishing, 2014, pp. 28–37. ISBN: 9783939897668. DOI: [10.4230/OASIcs.MCPS.2014.28](https://doi.org/10.4230/OASIcs.MCPS.2014.28).
- [50] Gabriela Ortiz-León et al. “An approximation of heart failure using cardiovascular simulation toolbox”. In: *Biomimetics* 4 (3 Sept. 2019). ISSN: 23137673. DOI: [10.3390/biomimetics4030047](https://doi.org/10.3390/biomimetics4030047).
- [51] Pierpaolo Pellicori et al. “Cardiac Dysfunction, Congestion and Loop Diuretics: their Relationship to Prognosis in Heart Failure”. In: *Cardiovascular Drugs and Therapy* 30 (6 Dec. 2016), pp. 599–609. ISSN: 15737241. DOI: [10.1007/s10557-016-6697-7](https://doi.org/10.1007/s10557-016-6697-7).
- [52] Piotr Ponikowski and Ewa A. Jankowska. “Pathogenesis and Clinical Presentation of Acute Heart Failure”. In: *Revista Española de Cardiología (English Edition)* 68 (4 Apr. 2015), pp. 331–337. ISSN: 18855857. DOI: [10.1016/j.rec.2015.02.001](https://doi.org/10.1016/j.rec.2015.02.001).
- [53] Ali Pourmand et al. “The utility of point-of-care ultrasound in the assessment of volume status in acute and critically ill patients”. In: *World Journal of Emergency Medicine* 10 (4 2019), p. 232. ISSN: 1920-8642. DOI: [10.5847/wjem.j.1920-8642.2019.04.007](https://doi.org/10.5847/wjem.j.1920-8642.2019.04.007).
- [54] Stephan Rosenkranz et al. *Left ventricular heart failure and pulmonary hypertension*. Mar. 2016. DOI: [10.1093/eurheartj/ehv512](https://doi.org/10.1093/eurheartj/ehv512).
- [55] Gesuele Adriano Salvitti Simone Russo Marianna. “Impatto delle patologie respiratorie croniche: gestione a lungo termine e ruolo della riabilitazione.” In: (2019). DOI: [10.36166/25314920-A082](https://doi.org/10.36166/25314920-A082)(<https://doi.org/10.36166/2531>).
- [56] David S. Shin et al. *The inferior vena cava: a pictorial review of embryology, anatomy, pathology, and interventions*. July 2019. DOI: [10.1007/s00261-019-01988-3](https://doi.org/10.1007/s00261-019-01988-3).
- [57] Cindy L. Stanfield. *Principles of Human Physiology - IV edition*. Pearson, Benjamin Cummings, 2011.
- [58] Jennifer T. Thibodeau and Mark H. Drazner. *The Role of the Clinical Examination in Patients With Heart Failure*. July 2018. DOI: [10.1016/j.jchf.2018.04.005](https://doi.org/10.1016/j.jchf.2018.04.005).
- [59] Burns B. Tucker WD Shrestha R. *Anatomy, Abdomen and Pelvis, Inferior Vena Cava*. 2022.

- [60] *Ultrasound imaging of congestion in heart failure: examinations beyond the heart*. May 2021. DOI: [10.1002/ejhf.2032](https://doi.org/10.1002/ejhf.2032).
- [61] Mauro Ursino. *Interaction between carotid baroregulation and the pulsating heart: a mathematical model*. 1998.
- [62] Adnan Yamanoglu et al. “The role of inferior vena cava diameter in the differential diagnosis of dyspneic patients; Best sonographic measurement method?” In: vol. 33. W.B. Saunders, 2015, pp. 396–401. DOI: [10.1016/j.ajem.2014.12.032](https://doi.org/10.1016/j.ajem.2014.12.032).
- [63] Xiuquan Zhang. *Cardiovascular System Modeling Using Modified Nodal Analysis and Trapezoidal Rule*.
- [64] Zhongheng Zhang et al. *Ultrasonographic measurement of the respiratory variation in the inferior vena cava diameter is predictive of fluid responsiveness in critically ill patients: Systematic review and meta-analysis*. 2014. DOI: [10.1016/j.ultrasmedbio.2013.12.010](https://doi.org/10.1016/j.ultrasmedbio.2013.12.010).